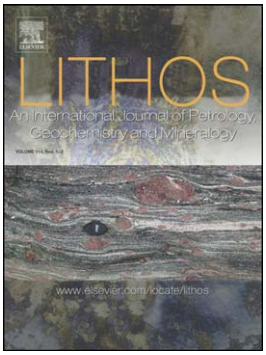

Origin and evolution of Cenozoic magmatism of Sardinia (Italy). A combined isotopic (Sr-Nd-Pb-O-Hf-Os) and petrological view

Michele Lustrino, Lorenzo Fedele, Leone Melluso, Vincenzo Morra, Fiorenzo Ronga, Jörg Geldmacher, Svend Duggen, Samuele Agostini, Ciro Cucciniello, Luigi Franciosi, Thomas Meisel

PII: S0024-4937(13)00285-5
DOI: doi: 10.1016/j.lithos.2013.08.022
Reference: LITHOS 3071

To appear in: *LITHOS*

Received date: 25 February 2013
Accepted date: 29 August 2013

Please cite this article as: Lustrino, Michele, Fedele, Lorenzo, Melluso, Leone, Morra, Vincenzo, Ronga, Fiorenzo, Geldmacher, Jörg, Duggen, Svend, Agostini, Samuele, Cucciniello, Ciro, Franciosi, Luigi, Meisel, Thomas, Origin and evolution of Cenozoic magmatism of Sardinia (Italy). A combined isotopic (Sr-Nd-Pb-O-Hf-Os) and petrological view, *LITHOS* (2013), doi: 10.1016/j.lithos.2013.08.022

Origin and evolution of Cenozoic magmatism of Sardinia (Italy). A combined isotopic (Sr-Nd-Pb-O-Hf-Os) and petrological view

Michele Lustrino[1,2,*], Lorenzo Fedele[3], Leone Melluso[3], Vincenzo Morra[3], Fiorenzo Ronga[3], Jörg Geldmacher[4], Svend Duggen[4,5], Samuele Agostini[6], Ciro Cucciniello[3], Luigi Franciosi[3], Thomas Meisel[7]

1 = Dipartimento di Scienze della Terra, Università degli Studi di Roma La Sapienza, P.le A. Moro, 5, 00185 Roma, Italy.

2 = CNR, Istituto di Geologia Ambientale e Geoingegneria (IGAG), c/o Dipartimento di Scienze della Terra, Università degli Studi di Roma La Sapienza, P.le A. Moro, 5, 00185 Roma, Italy.

3 = Dipartimento di Scienze della Terra, dell'Ambiente e delle Risorse, Università degli Studi di Napoli Federico II, Via Mezzocannone, 8, 80134, Napoli, Italy.

4 = GEOMAR - Helmholtz Centre for Ocean Research Kiel, Wischhofstr. 1-3, 24148 Kiel, Germany.

5 = A.P. Møller Skolen in Schleswig, Upper Secondary School and Sixth Form College of the Danish National Minority in Northern Germany.

6 = CNR - Istituto di Geoscienze e Georisorse, Via Giuseppe Moruzzi,1 56124 Pisa, Italy

7 = Montanuniversität Leoben, 120 Lehrstuhl für Allgemeine und Analytische Chemie, 8700 Leoben, Franz-Josef-Straße 18 (AACH), Leoben, Austria.

* = corresponding author. E-mail: michele.lustrino@uniroma1.it

ABSTRACT

The Cenozoic igneous activity of Sardinia is essentially concentrated in the 38-0.1 Myr time range. On the basis of volcanological, petrographic, mineralogical, geochemical and isotopic considerations, two main rock types can be defined. The first group, here defined SR (Subduction-Related) comprises Late Eocene-Middle Miocene (~38-15 Ma) igneous rocks, essentially developed along the Sardinian Trough, a N-S oriented graben developed during the Late Oligocene-Middle Miocene. The climax of magmatism is recorded during the Early Miocene (~23-18 Ma) with minor activity before and after this time range. Major and trace element indicators, as well as Sr-Nd-Pb-Hf-Os-O isotope systematic indicate complex petrogenetic processes including subduction-related metasomatism, variable degrees of crustal contamination at shallow depths, fractional crystallization and basic rock partial melting. Hybridization processes between mantle and crustal melts and between pure mantle and crustally contaminated mantle melts increased the isotopic and elemental variability of the composition of the evolved (intermediate to acid) melts. The earliest igneous activity, pre-dating the Early Miocene magmatic climax, is related to the pushing effects exerted by the Alpine Tethys over the Hercynian or older lower crust, rather than to dehydration processes of the oceanic plate itself.

The second group comprises volcanic rocks emplaced from ~12 to ~0.1 Ma. The major and, partially, trace element content of these rocks roughly resemble magmas emplaced in within-plate tectonic settings. From a Sr-Nd-Pb-Hf-Os isotopic point of view, it is possible to subdivide these rocks in two subgroups. The first, defined RPV (Radiogenic Pb Volcanic) group comprises the oldest and very rare products (~12-4.4 Ma) occurring only in the southern sectors of Sardinia. The second group, defined UPV (Unradiogenic Pb Volcanic), comprises rocks emplaced in the remaining central and northern sectors during the ~4.8-0.1 Ma time range. The origin of the RPV rocks remains quite enigmatic, since they formed just a few Myr after the end of a subduction-related igneous activity but do not show any evidence of slab-derived metasomatic effects. In contrast, the complex origin of the mafic UPV rocks, characterized by low $^{206}Pb/^{204}Pb$ (17.4-18.1), low $^{143}Nd/^{144}Nd$ (0.51232-0.51264), low $^{176}Hf/^{177}Hf$ (0.28258-0.28280), mildly radiogenic $^{87}Sr/^{86}Sr$ (~0.7044) and radiogenic $^{187}Os/^{188}Os$ ratios (0.125-0.160) can be explained with a mantle source modified after interaction with ancient delaminated lower crustal lithologies. The strong isotopic difference between the RPV and UPV magmas and the absence of lower crustal-related features in the SR and RPV remain aspects to be solved.

INTRODUCTION

During the Cenozoic, a widespread igneous activity developed in the Mediterranean area, mostly within the Alpine suture zone and partially along the older Variscan suture in central Europe (e.g., Duggen et al., 2005; Harangi et al., 2006; Lustrino and Wilson, 2007; Lustrino et al., 2011; Carminati et al., 2012, and references therein). Most of the volcanological, mineralogical and geochemical features observed in the various circum-Mediterranean igneous districts are well represented in the island of Sardinia, which is thus a key-locality for magmatic and geodynamic studies on the basis of several considerations:

1) The island acted as the foreland of the earlier Alpine Orogeny and the hinterland of the Apennine subduction system (e.g., Carminati et al., 2012).

2) In Sardinia two different igneous phases developed during the Cenozoic, the oldest (Late Eocene-Middle Miocene) is considered to be related to the originally NW-directed Apennine subduction system, whereas the youngest (Middle Miocene-Quaternary) volcanism seems geochemically unrelated to active or recent subduction processes (e.g., Lustrino et al., 2007a, 2009, 2011; Fig. 1).

3) The igneous rocks, essentially in volcanic facies, cover about one fourth of the island (Fig. 1), making their investigation relatively easy and statistically relevant.

4) The most recent “anorogenic” products often carry mantle xenoliths, therefore providing direct evidence on the composition of the local shallow sub-continental mantle (e.g., Rocco et al., 2012, and references therein).

5) More than 99% of the “anorogenic” products show unique geochemical compositions compared to the rest of the “anorogenic” lavas of the circum-Mediterranean area in terms of BSE-like Sr, sub-chondritic Nd and very low $^{206}Pb/^{204}Pb$ isotopes (e.g., Lustrino et al., 2007a).

Former studies have evidenced the peculiar isotopic composition of the Cenozoic igneous rocks of Sardinia, even though a comprehensive Sr-Nd-Pb-Hf-Os-O isotopic study is still missing. This paper presents thirty-four new Sr-, thirty new Nd-, thirty new Pb-, seventeen new Hf-, seven new Os- and fifteen new O-isotopic ratios for the most representative samples of both "orogenic" and "anorogenic" rocks. Our new results are integrated with published and new major- and trace-element and isotopic data of Sardinian rocks, in order to examine the petrological and geodynamic processes associated with their origin.

GEOLOGICAL BACKGROUND AND MAGMATIC EVOLUTION

The geological setting and background of the island of Sardinia has been recently reviewed (e.g., Lustrino et al., 2009, 2011; Carminati et al., 2010, 2012) and for this reason only the most important aspects will be summarized here. Until the Oligocene, Sardinia and Corsica were part of the southern European paleo-margin. After a NE-SW striking rifting stage, mostly developed during the Oligocene, a ~55-60° Early Miocene counter-clockwise rotation separated the Sardinia-Corsica block from Europe (~22-15 Ma; Fig. 2; Gattacceca et al., 2007; Carminati et al., 2010, 2012, and references therein). A branch of this rifting system is now identified in the Sardinian Trough (*Fossa Sarda* in the Italian literature), a ~220 km-long, ~40 km-wide middle Oligocene-Aquitanian rift system cutting the island from north to south (Lecca et al., 1997; Faccenna et al., 2002; Cherchi et al., 2008; Fig. 1). During the Langhian (~15 Ma) the Sardinia-Corsica block rotation ceased, thereby attaining its roughly N-S oriented present position (e.g., Vigliotti and Langenheim, 1995; Speranza et al., 2002; Gattacceca et al., 2007). The rotation of the Sardinia-Corsica block was associated with the opening of the Ligurian-Provençal back-arc basin and was roughly coeval also with the clockwise rotation of the Balearic Promontory and the opening of the Valencia Trough (Fig. 2). The peak of the angular velocity coincided with the peak of magma productivity, whereas the end of the Sardinia-Corsica rotation coincided with the end of the "orogenic" igneous activity. After few Myr of quiescence, Sardinia was affected by a reprise of igneous activity from early Late Miocene (~12 Ma) to Pleistocene (~0.1 Ma), with a peak concentrated around Middle-Late Pliocene (Beccaluva et al., 1985; Lustrino et al., 2000, 2004a, 2007a, 2007b, and references therein).

The origin of the Oligo-Miocene extensional movements recorded in the western Mediterranean basins has been related to the gravitative sinking of subducted oceanic lithosphere of the Tethyan Ocean (Ionian Sea) subducting north-westward since late Eocene, possibly coupled with an asthenospheric east-directed mantle flow (e.g., Alvarez, 1974; Beccaluva et al., 1989; Gueguen et al., 1998; Carminati et al., 2012). The oldest igneous rocks (~38 Myr; Lustrino et al., 2009; Fig. 3) are represented by a small microdiorite body from Calabona area (N Sardinia). Late Eocene-Late Oligocene igneous activity in Sardinia was sporadic, with the bulk of the orogenic igneous activity starting around 28 Ma (Lecca et al., 1997), and peaking during the 22-18 Myr time range (Beccaluva et al., 1985; Speranza et al., 2002; Gattacceca et al., 2007; Carminati et al., 2012, and

references therein; Fig. 3). Rock compositions are mostly intermediate to acid subalkaline terms (essentially basaltic andesites, andesites, dacites and rhyolites), mainly resulting from explosive activity (mostly ignimbritic flows), with rare mildly alkaline compositions (shoshonites and latites) and very rare basic-ultrabasic exceptions (e.g., basalts and picritic basalts of Montresta and Arcuentu, north-western and south-western Sardinia, respectively; Morra et al., 1997; Brotzu et al., 1997b; Downes et al., 2001; Franciosi et al., 2003; Beccaluva et al., in press). Trace element abundances and isotopic ratios of the less differentiated Late Eocene-Middle Miocene rocks led several authors to propose a derivation from a mantle wedge modified by slab-derived fluids (e.g., Morra et al., 1997; Mattioli et al., 2000; Downes et al., 2001; Franciosi et al., 2003; Lustrino et al., 2009; Conte et al., 2010; Guarino et al., 2011).

The Serravalian (~11.8 Ma) volcanic rocks of the Isola del Toro (SW Sardinia) mark an abrupt change in terms of chemistry, petrography and volcanological facies compared with the older igneous activity (Lustrino et al., 2007a, 2007b, 2009). After a ~5 Myr quiescence, the volcanic activity continued in the southern sector of Sardinia only (Capo Ferrato, Rio Girone and Guspini; Lustrino et al., 2000; 2007a). The volcanic rocks produced during the ~11.8-4.4 Ma time span define the so-called RPV (Radiogenic Pb Volcanic) group (Lustrino et al., 2000; Figs. 1, 3). They share major and trace element content and ratios, as well as Sr-Nd-Pb isotopic ratios with the other anorogenic rocks of the CiMACI (Circum-Mediterranean Anorogenic Cenozoic Igneous) Province (Lustrino and Wilson, 2007; Lustrino, 2011).

From Early Pliocene to Quaternary (~4.8-3.9-0.1 Ma), the volcanic activity developed in the remaining central and northern sectors of the island (Oristano Gulf, Gerrei, Abbasanta-Planargia-Paulilatino Plains, Orosei-Dorgali, Mt. Arci, Logudoro; Cioni et al., 1982; Montanini et al., 1994; Lustrino et al., 1996, 2002, 2004a, 2004b, 2007a; Gasperini et al., 2000; Fedele et al., 2007; Duncan et al., 2011; Kim et al., 2011; Figs. 1, 3). The volcanic rocks belonging to this phase define the UPV (Unradiogenic Pb Volcanic) group (Lustrino et al., 2000), characterized by peculiar trace element and Sr-Nd-Pb isotopic composition compared to the rest of the CiMACI products (Lustrino and Wilson, 2007).

To resume, the Cenozoic igneous rocks of Sardinia can be grouped in three major types (Fig. 1, 3): 1) a Late Eocene-Middle Miocene (~38-15 Ma) group with subduction-related geochemical and petrographic characteristics (hereafter SR, Subduction-Related); 2) a very rare late Middle

Miocene-Early Pliocene group, cropping out in southernmost Sardinia only, with sodic alkaline composition resembling typical anorogenic magma (RPV) and 3) an abundant Middle Pliocene-Middle Pleistocene (~4.8-0.1 Ma) group (UPV), cropping out in central and northern Sardinia, with major element contents resembling typical sodic alkaline to tholeiitic anorogenic magma, but with absolutely unique trace element and Sr-Nd-Pb isotopic characteristics.

SAMPLE DESCRIPTION

A total of sixty samples have been investigated in this study for Sr-Nd-Pb-O-Hf-Os isotopic analyses, selected from a database of over 600 rocks collected during the last twenty years. Eighteen samples from the least evolved compositions (basalts to basaltic andesites) plus twenty-three from the most evolved (dacites to rhyolites) were selected for the Late Eocene-Middle Miocene SR phase. Eight RPV and eleven UPV samples complete the selected dataset.

All the SR rocks fall in the subalkaline field as defined by Le Maitre (2005), and show Ti-poor (TiO_2 <1.1 wt%), P-poor (P_2O_5 <0.3 wt%) and Ca-rich compositions (CaO up to 12.8 wt%) covering the entire range from basalt to rhyolite (Fig. 4). Only a small group of rocks from northern Sardinia (Anglona) straddle the subalkaline-mildly alkaline field, reaching shoshonitic and latitic compositions (Beccaluva et al., in press). Despite being classically ascribed to the calcalkaline rock association, the SR rocks do not show the typical Fe-poor composition, with Fe_2O_{3tot} reaching 12.1 wt% (Conte et al., 2010). Following Miyashiro (1974), less than one half of the SR rocks are calcalkaline (i.e., plot below the dashed line in Fig. 5), whereas, according to Arculus (2003), the SR rocks should better defined as medium- to high-Fe types, with only a minor group of samples plotting in the low-Fe field (Fig. 5).

Rocks of the RPV group range in composition from trachybasalt to trachyte and show a mildly Na-alkaline serial affinity. The bulk of the UPV samples cluster in a relatively restricted field between trachybasalt and basaltic trachyandesite (Fig. 4). These rocks show two distinct differentiation trends, one pointing towards the phonolitic minimum (Montiferro) and the other pointing towards the rhyolitic minimum (Mt. Arci; Figs. 1, 4). The subordinate tholeiitic basalts of the UPV group are present throughout the island, whereas dacitic to rhyolitic compositions are confined in the Mt. Arci district only.

ISOTOPIC COMPOSITION

Strontium isotope ratios

The SR igneous rocks of Sardinia show a wide range of $^{87}Sr/^{86}Sr$ initial isotopic composition (0.7036-0.7113; Table 1, Fig. 6a), with no clear correlation with MgO contents (Fig. 7a). A crude positive correlation exists between $^{87}Sr/^{86}Sr$ and SiO_2 for the basic-intermediate compositions (Fig. 7b). This is particularly clear for the Montresta igneous rocks showing a good $^{87}Sr/^{86}Sr$-SiO_2 correlation ($R^2 = 0.84$) and a poor negative $^{87}Sr/^{86}Sr$-MgO correlation ($R^2 = 0.31$; Table 1). The most silica-poor rocks (SiO_2 = 45.1-50.1 wt%) are characterized by the least radiogenic compositions ($^{87}Sr/^{86}Sr$ = 0.7040-0.7047). The highest $^{87}Sr/^{86}Sr$ ratios (>0.710) are measured in the most evolved samples from the Arcuentu volcanic complex (SiO_2 ~55-58 wt%). Interestingly, a general decrease of $^{87}Sr/^{86}Sr$ with increasing SiO_2 is observed for SiO_2 values >66 wt% (Fig. 7b).

Middle Miocene-Quaternary volcanic rocks (RPV and UPV groups) as a whole show a larger $^{87}Sr/^{86}Sr$ isotopic range, from 0.7031 to 0.7153 (Table 1, Fig. 6a). The least differentiated RPV rocks (MgO = 7.6-4.2 wt %) show relatively low but variable Sr isotopic ratios ($^{87}Sr/^{86}Sr$ = 0.7031-0.7044), whereas the most differentiated (benmoreites and trachytes from Isola del Toro; MgO = 3.0-0.1 wt %) are characterized by higher $^{87}Sr/^{86}Sr$ (0.7048-0.7054; Lustrino et al., 2007b; Fig. 7a). With the exception of the most differentiated samples from Mt. Arci (dacites and rhyolites; SiO_2 >63 wt %; MgO <2.5 wt%), showing extremely radiogenic $^{87}Sr/^{86}Sr$ (0.7072-0.7155; Fig. 7b) all the remaining UPV samples (MgO = ~11-3 wt%) mostly fall in the 0.7042-0.7051 range, with an average $^{87}Sr/^{86}Sr$ of 0.7044 ± 0.0002 (Fig. 7a,b). The differentiated samples from Mt. Arci have clear petrographic, geochemical and isotopic characteristics that speak for a crustal anatectic origin or an hybrid origin resulting after the mixing of mantle and crustal melts (e.g., Montanini et al., 1994), and for this reason these will be no more treated in this study.

Neodymium isotope ratios

Similarly to what seen for Sr isotope ratios, the Sardinian SR volcanic rocks show a wide range of $^{143}Nd/^{144}Nd$ initial values, from 0.51218 to 0.51274 (Table 1; Fig. 6a). The $^{143}Nd/^{144}Nd$ ratios show a good negative correlation with SiO_2 ($R^2 = 0.80$) from ~47 to ~58 wt% SiO_2 which then inverts at

higher SiO_2 (Fig. 7d). A similar correlation, albeit with larger spread of data, is observed also between $^{143}Nd/^{144}Nd$ and MgO (Fig. 7c).

The RPV rocks show the most radiogenic Nd isotopic composition among the Cenozoic igneous rocks of Sardinia ($^{143}Nd/^{144}Nd$ = 0.51271-0.51289; Fig. 6a). Differently from what observed for $^{87}Sr/^{86}Sr$, the UPV group shows a wide range in $^{143}Nd/^{144}Nd$ (0.51263-0.51216 Table 1; Fig. 6a). The most evolved samples of Mt. Arci, characterized by high Sr-radiogenic ratios, are confined to the most Nd unradiogenic compositions ($^{143}Nd/^{144}Nd$ = 0.51216-0.51228). $^{143}Nd/^{144}Nd$ values for both RPV and UPV groups show negative trends with SiO_2 (R^2 = 0.61 and 0.81, respectively; Fig. 7d) and a slightly positive trends with MgO (R^2 = 0.54 and 0.64, respectively; Fig. 7c).

Lead isotope ratios

The SR rocks show relatively uniform uranogenic Pb isotopic ratios (average $^{206}Pb/^{204}Pb$ = 18.67 ± 0.097 at 2σ level; $^{207}Pb/^{204}Pb$ = 15.64 ± 0.022) and slightly more variable thorogenic Pb isotopic ratios ($^{208}Pb/^{204}Pb$ = 38.72 ± 0.112; Fig. 6b,c). The relative homogeneity of the Pb isotopic ratios strongly contrasts with the variability in $^{87}Sr/^{86}Sr$ and $^{143}Nd/^{144}Nd$ (0.7036-0.7076 and 0.51218-0.51274, respectively; Fig. 6d,e).

The two new Pb isotopic ratios for RPV presented here ($^{206}Pb/^{204}Pb$ = 18.94; $^{207}Pb/^{204}Pb$ = 15.62; $^{208}Pb/^{204}Pb$ = 38.72; Isola del Toro) fall within the field of the previous RPV literature (Lustrino et al., 2000) and the field of the CiMACI rocks (Lustrino and Wilson, 2007). No new data are presented on UPV rocks because these rocks have been already fully investigated, with 23 Pb isotopic ratios being available in literature (Gasperini et al., 2000; Lustrino et al., 2000, 2002, 2007a). The UPV rocks have Pb isotopic compositions that find no counterparts in the CiMACI Province ($^{206}Pb/^{204}Pb$ = 17.51-18.07; $^{207}Pb/^{204}Pb$ = 15.53-15.62; $^{208}Pb/^{204}Pb$ = 37.66-38.33; Fig 6c-e).

Oxygen isotope ratios

Oxygen isotopic data were obtained by laser fluorination technique for five SR samples (Table 1). Where possible, separates of fresh olivine were analyzed (Montresta and Arcuentu samples); otherwise, clinopyroxene was chosen (Marmilla). $\delta^{18}O_{ol}$ of Montresta samples are lower (+5.41 and +5.58‰) than those of Arcuentu samples (+6.21 and +6.43‰; Table 1). Considering the oxygen

isotopic fractionation between olivine and clinopyroxene ($\delta^{18}O_{cpx} = \delta^{18}O_{ol}$ + 0.4‰ at ~1000-1200 °C; Chiba et al., 1989; Zheng, 1993; Mattey et al., 1994; Baker et al., 2000; Duggen et al., 2008), the $\delta^{18}O_{ol}$ of Arcuentu samples (corresponding to $\delta^{18}O_{cpx}$ +6.6 to 6.8‰) fall in the same compositional range reported by Downes et al. (2001) for clinopyroxene phenocrysts (from +6.1‰ to + 7.4‰). The clinopyroxene separates from Marmilla gave higher $\delta^{18}O_{cpx}$ (+7.02‰, corresponding to $\delta^{18}O_{ol}$ +6.6‰; Table 1).

Due to the aphyric to sparsely plagioclase-olivine phyric texture, oxygen laser fluorination analyses of UPV and RPV samples have been performed essentially on plagioclase and only subordinately on clinopyroxene and olivine separates. Ten $\delta^{18}O$ mineral analyses (each analysis run in duplicate or triplicate) gave a wide range of composition, from +6.46 to +10.24‰ (Table 1). Only two RPV samples have been analyzed for oxygen isotopes, both belonging to the Capo Ferrato district (SE Sardinia). The less differentiated Capo Ferrato rock (mugearite MAL3; MgO = 4.24 wt%) show the lowest $\delta^{18}O_{ol}$ (+5.43‰; corresponding to $\delta^{18}O_{cpx}$ +5.8‰). For the other Capo Ferrato sample (trachyte CF; MgO = 1.26 wt%) it was possible to separate only feldspar phenocrysts, characterized by much higher $\delta^{18}O$ (+7.17‰). The UPV $\delta^{18}O_{ol}$ values, measured in separates from Montiferro, Orosei-Dorgali and Santu Lussurgiu lavas, range from +5.37‰ to +5.98‰ (corresponding to $\delta^{18}O_{cpx}$ +5.8‰ to +6.4‰). The UPV $\delta^{18}O_{cpx}$ values, measured in Montiferro and Capo Frasca rocks, are generally slightly higher, ranging from +5.41‰ (phonolite GFP89 from Montiferro, with MgO = 0.87 wt%) to +6.74‰ (basaltic andesite MAL32 from Capo Frasca with MgO = 6.26 wt%). The single $\delta^{18}O_{pl}$ value, measured in a Gerrei hawaiite, is +6.67‰.

Hafnium isotope ratios

Seven among the most primitive SR samples from Montresta, Arcuentu, Marmilla, Cuguttada and Capo Frasca were selected for Hf isotope analyses, the first ever published for the Late Eocene-Middle Miocene igneous rocks of Sardinia. $^{176}Hf/^{177}Hf$ ratios are relatively radiogenic and range from 0.28278 (Cuguttada basalt) to 0.28302 (Capo Frasca basalt; Table 1).

The $^{176}Hf/^{177}Hf$ ratios measured for the RPV group (Capo Ferrato, Rio Girone, Guspini and Isola del Toro) vary from 0.28286 to 0.28304 (Table 1; Fig. 6f), falling in the range of SR rocks (Fig. 6f). The five analyses reported here for the UPV rocks (Mt. Arci, Montiferro, Orosei-Dorgali, Capo Frasca and Gerrei) are much less radiogenic than the RPV samples and fall, enlarging, into the

$^{176}Hf/^{177}Hf$ field (0.28258-0.28279; Table 1; Fig. 6f) previously defined by Gasperini et al. (2000). $^{176}Hf/^{177}Hf$ ratios show strong positive correlation with Nd isotopes, a less distinct positive correlation with Pb isotopes and no apparent correlation with the $^{87}Sr/^{86}Sr$ isotopic system (Fig. 6f-h).

Osmium isotope ratios

The Osmium isotopic ratios presented here are the first ever measured for the Cenozoic igneous rocks of Sardinia and among the very few analyses available for both the "orogenic" and the "anorogenic" igneous rocks of the circum-Mediterranean area (see discussion paragraph). One of the problems regarding Os isotope systematic of igneous rocks is the very low content of this element (generally present in ppb to ppt concentration levels), resulting in a very easy modification of the isotopic ratio after interaction with crustal lithologies *en route* to the surface.

Among the SR rocks, only one sample (MAL35) was successfully analyzed for Os isotopes. The MAL35 sample from Capo Frasca shows relatively low $^{187}Os/^{188}Os$ (0.1317; Table 1), considering its Sr radiogenic and Nd unradiogenic composition ($^{87}Sr/^{86}Sr$ = 0.70552; $^{143}Nd/^{144}Nd$ = 0.51268). This Os isotopic composition of the SR rock is lower than the range of the other Cenozoic subduction-related rocks from the circum-Mediterranean area (Peninsular Italy; Conticelli et al., 2007), characterized by $^{187}Os/^{188}Os$ ranging from 0.1372 to 0.5813. Two RPV samples (Guspini and Rio Girone) and seven UPV samples (Mt. Arci, Orosei-Dorgali and Gerrei) have been analyzed for Os isotopes. The two RPV samples show $^{187}Os/^{188}Os$ (0.1842-0.1983) much more radiogenic than MAL35 sample and more radiogenic than the UPV samples ($^{187}Os/^{188}Os$ = 0.1255-0.4230; Table 1). With the exception of two radiogenic Os samples ($^{187}Os/^{188}Os$ = 0.2945-0.4230), the bulk of the UPV rocks show similarities with the only SR rock analyzed ($^{187}Os/^{188}Os$ = 0.1255-0.1583; Table 1). Excluding the two Os radiogenic UPV samples (MGL223 and MGV236A), the Os isotopic composition of the Sardinian rocks shows crude negative trends with $^{87}Sr/^{86}Sr$ and positive correlation with $^{143}Nd/^{144}Nd$, $^{206}Pb/^{204}Pb$, $^{207}Pb/^{204}Pb$, $^{208}Pb/^{204}Pb$ and $^{176}Hf/^{177}Hf$, even if with some scatter (Fig. 8). The two ^{187}Os-rich samples have been discounted because they show the lowest elemental Os content (0.011-0.030 ppb), a feature that renders them easily prone to isotopic variation as consequence of alteration or contamination during ascent. Among the other CiMACI Province rocks, only those from the German volcanic districts (Bad Urach, Hegau, Rhon,

Vogelsberg; Jung et al., 2005, 2011; Pfander et al., 2012) have been fully analyzed for Os isotope systematic too (Fig. 8). Compared with these rocks, the UPV show complete overlap of values, even if the Sardinian rocks are shifted towards much higher $^{87}Sr/^{86}Sr$, lower $^{143}Nd/^{144}Nd$, lower $^{206}Pb/^{204}Pb$ and lower $^{176}Hf/^{177}Hf$.

DISCUSSION

Origin and evolution of SR rocks

The Late Eocene-Middle Miocene magmatism (~38-15 Ma) of Sardinia with subduction-related geochemical characteristics is classically interpreted as related with the NW-directed subduction system that started to consume ancient oceanic lithosphere of the Tethys Ocean (e.g., Beccaluva et al., 1989; Gueguen et al., 1998; Lustrino et al., 2009; Carminati et al., 2012).

From a Sr-Nd isotopic point of view, the SR rocks of Sardinia reflect the involvement of at least two components. One end-member could be a DMM- (Depleted MORB Mantle) like source, variably modified by a second component, more radiogenic in Sr and unradiogenic in Nd, as already quantified by Franciosi et al. (2003). This second component could be represented by the recycled sediments and/or the oceanic crust itself of the eastern branch of the Alpine Tethys. Alternatively, at least some of the Sr-Nd isotopic heterogeneity could be related to shallow-level processes of crustal interaction, as proposed by other authors (e.g., Morra et al., 1994, 1997; Brotzu et al., 1997a, 1997b; Conte, 1997; Lonis et al., 1997; Conte et al., 2010).

The Sr-Nd isotope variation with major element differentiation indexes (i.e., SiO_2, MgO) is particularly complex. Some igneous districts (e.g., Montresta, reported with the same symbol as all the remaining SR rocks for the sake of clarity) show clear correlations of $^{87}Sr/^{86}Sr$ with SiO_2 and MgO ($R^2 = 0.93$ in both cases; Fig. 7; Table 1). A particularly interesting feature is represented by the upward convex $^{87}Sr/^{86}Sr$ vs. SiO_2 and downward convex $^{143}Nd/^{144}Nd$ vs. SiO_2 variations, with a major change observed at ~58-62 wt% SiO_2 (Fig. 7b,d). The Logudoro-Bosano and the Sulcis volcanic rocks better than all the others define such an anomalous trend (again reported with the same symbol as the rest of the SR rocks). The Sr-Nd isotopic variation with MgO is nearly the opposite to what observed with SiO_2, but with less clear trends. Mildly evolved compositions (~6-6.5 wt% MgO) are characterized by a large spread of both $^{87}Sr/^{86}Sr$ (0.7043-0.7108) and

$^{143}Nd/^{144}Nd$ (0.5126-0.5122), testifying for complex processes of crustal interaction at shallow levels and/or mantle depths.

Figure 9 shows the mixing line between a DMM-like source and Atlantic Ocean-type sediments. The Sr-Nd isotopic composition of the most mafic SR rocks (e.g., sample KB23 from Montresta) can be produced adding less ~1.5% sediments to a DMM-like mantle. If, instead of using the bulk sediment, we assume addition of sediment-derived fluids, the amount of crustal material necessary to explain the SR isotopic composition reduces to 0.1-0.5% (Franciosi et al., 2003). Assimilation of a subducted sediment component is also consistent with the observed trends towards higher $^{207}Pb/^{204}Pb$ isotope ratios (at nearly constant $^{206}Pb/^{204}Pb$ ratios) and towards lower $^{176}Hf/^{177}Hf$ ratios (with decreasing $^{143}Nd/^{144}Nd$ ratios). The isotopic vectors point towards compositions much more extreme than typical EM-II end-member (Enriched Mantle type II composition; Zindler and Hart, 1986), commonly believed to represent the involvement of terrigenous subducted sediments in intra-plate oceanic basalts (OIBs).

The effects of interaction between a basaltic melt and the basement rocks were modelled using two mixing lines using literature data from Hercynian basic to acid igneous rocks (Fig. 9). The much higher Sr and Nd content of KB23 sample (compared with a DMM source) requires much higher amounts of digestion of Hercynian rocks in order to record a significant Sr-Nd isotopic shift. The mixing lines between KB23 sample and two of the most extreme Hercynian rocks are reported in Fig. 9, indicating that such kind of interaction could in theory produce the entire Sr-Nd isotopic variation of the SR rocks of Sardinia. What seems unlikely is the extremely high amount of basement rock that should be digested (typically >20%, up to ~80%) in order to reach the most evolved isotopic compositions.

In summary, both the processes of sediment recycling and shallow depth melt contamination can explain the Sr-Nd isotopic range of the SR igneous rocks. Anyway, the process of fractional crystallization would produce porphyritic textures, a feature in contrast with the vitreous to poorly-phyric petrography of much of the Sardinian ignimbrites. We consider this as evidence against assimilation plus fractional crystallization processes involving digestion of large amounts of basement rocks. Moreover, the wide spectrum of Sr-Nd isotopic composition at a given MgO is more compatible with source heterogeneity where the isotopic compositions are decoupled from the MgO content of the cooling partial melt.

The convex upward and downward correlations of $^{87}Sr/^{86}Sr$ with SiO_2 and MgO are not consistent with a simple model of crustal contamination. Here we propose that the most differentiated rocks (SiO_2 >63 wt%; MgO <2.5 wt%) derive from partial melting of the most mafic, basic, lithologies. Low degrees of melting of the early crystallized basaltic/gabbroic SR compositions would in fact produce high SiO_2 and low MgO melts, as experimentally demonstrated in several cases (e.g., Rapp and Watson, 2005; Qian and Hermann, 2013, and references therein). Increasing degrees of partial melting of an isotopically homogeneous basaltic/gabbroic source could produce liquids with increasing MgO and decreasing SiO_2 content (e.g., Qian and Hermann, 2013), but without any concomitant isotopic shift. The existence of positive correlation between $^{87}Sr/^{86}Sr$ and SiO_2, as well as negative correlation between $^{143}Nd/^{144}Nd$ and SiO_2 (in rocks with SiO_2 >63 wt% and MgO <2.5 wt%) are thus interpreted as mixing trajectories. The end-member of this mixing process are 1) silica-rich partial melts of basaltic/gabbroic SR rocks, characterized by isotopic compositions in equilibrium with the most basic SR rocks, and 2) mildly evolved crustally contaminated (both in terms of source region and as partial melts) melts with andesitic s.l. composition (SiO_2 ~58 wt% and MgO ~2 wt%; Fig. 7b,d).

The convex patterns observed in Fig. 7b,d can be, therefore, explained with a multi-stage process involving: 1) production of subduction-related magma with relatively low $^{87}Sr/^{86}Sr$ and high $^{143}Nd/^{144}Nd$ (similar to what observed in Montresta); 2) variable degrees of crustal contamination associated with fractional crystallization to produce the mildly evolved compositions (e.g., SiO_2 56-60 wt%; arrow 1 in Figs. 7b,d); 3) partial melting of the early crystallized basaltic rocks at crustal levels, producing the silica-richest compositions with the same Sr-Nd isotopic ratios of the most basic-mafic terms (arrow 2 in Figs. 7b,d); 4) interaction between the silica-rich (SiO_2 >74 wt%) and magnesia-poor (MgO <1 wt%) melts produced during stage 1 with the crustally contaminated melts produced during stage 2 (arrow 3 in Figs. 7b,d). The general scheme of magma production requires four main stages of evolution: formation of an early "andesitoid" formation, followed by a "trachytoid" sequence, overlapped by a second "andesitoid" formation, and finally covered by the last "trachytoid" formation (Coulon et al., 1977). This sequence has been observed in the huge formations of the Bosano-Logudoro area as well as in the Sulcis district (Morra et al., 1994; Lecca et al., 1997; Conte et al., 2010; Guarino et al., 2011; Ronga, 2011). Such an alternation could be interpreted according to a model where the first "basaltic-andesitic" magmatism produces the lower

"andesitoid" sequence. Partial melting of the sub-surface lithologies, favoured by the passive increase of the isotherms due to the adiabatic upwelling of the lithosphere-asthenosphere boundary during the beginning of the counter clock-wise rotation of Sardinia would have produced the lower "trachytoid" (actually dacitic to rhyolitic) sequence. The increase of the angular velocity of Sardinia would have allowed dense basaltic melt to reach the surface along normal faults (e.g., Morra et al., 1997; Mattioli et al., 2000). During the last phases of rotation, the arrival of partial melts generated by passive upwelling of sub-lithospheric magma could have induced strong thermal perturbations, favouring the production of highly differentiated melts representing the upper "trachytoid" sequence of Coulon (1977).

The incompatible trace element abundance and ratios (e.g., low Nb-Ta, high LILE/HFSE ratios, high Pb) confirm the typical subduction-related geochemical characteristics (e.g., Duggen et al., 2005; Avanzinelli et al., 2009; Lustrino et al., 2011; Fig. 10a). The faintly LREE-enriched and HREE-flattened chondrite-normalized patterns additionally point to a spinel-bearing mantle source (Brotzu et al., 1997b; Morra et al., 1997; Franciosi et al., 2003; Lustrino et al., 2009).

The $\delta^{18}O_{ol}$ of the Montresta rocks reported here are only slightly higher than the average value of olivine in lithospheric mantle xenoliths and MORB (~+5.2‰; e.g., Mattey et al., 1994; Eiler et al., 1997). This is consistent with only limited amount of interaction between the (DMM-like) upper mantle beneath Montresta and the recycled subducted component, as already proposed by Franciosi et al. (2003) on the basis of Sr-Nd-Pb isotopic and incompatible element ratios.

Middle Miocene-Quaternary rocks (UPV and RPV)

The post-15 Myr volcanic products of Sardinia have geochemical characteristics resembling anorogenic magmas. We underline that the use of the adjective "anorogenic" for magmas temporally and geographically associated with subduction tectonics and subduction-related igneous activity is a risk and should be used with care. In most cases, the isotope systematic of magmas emplaced in mid-plate oceanic or continental settings requires an involvement of recycled lithologies (e.g., Lustrino, 2011, and references therein). At the same time, magmas defined as "anorogenic" from a geochemical point of view can be associated with recent or coeval subduction and continent-continent collision, or generated along ancient suture zones. This means that

adjectives such as “anorogenic” or “within-plate” used by geochemists and petrologists cannot be automatically exported into geological contexts and used for tectonic reconstructions (e.g., Lustrino and Wilson, 2007).

To address this issue, we have plotted in Figs. 10b,c the primitive mantle-normalized diagrams for the most mafic RPV and UPV samples together with the least differentiated basaltic rocks of St. Helena Island (Central Atlantic Ocean). The basalts of this island, together with those from other few localities in French Polynesia (Rurutu and Rarotonga islands; SW Pacific Ocean) define the HIMU-OIB type-locality, one of the geochemical end-member of the mantle “zoo”, believed to represent ancient, recycled oceanic crust (Zindler and Hart, 1986; Stracke et al., 2005; White, 2010; Stracke, 2012).

The RPV lavas show interelemental relationships closely resembling the St. Helena rocks. The only difference (trough at Ti) is likely due to fractionation of Fe-Ti opaque minerals in RPV, considering their relatively evolved composition (MgO 7.55-1.53 wt%). The RPV lavas are more compositionally similar to other CiMACI rocks than the UPV are (Lustrino, 2011). In particular, the Sr-Nd isotopic ratios of RPV rocks point toward the HIMU end-member and the FOZO (Focus Zone; Stracke et al., 2005) component. These compositions are generally absent from subduction-related magmas and are essentially present in mid-plate settings (more rarely also along oceanic ridges; Stracke et al., 2005). When considering the Pb isotopes, the RPV rocks plot along a line connecting St. Helena rocks (high $^{206}Pb/^{204}Pb$ and $^{143}Nd/^{144}Nd$, low $^{207}Pb/^{206}Pb$, $^{208}Pb/^{206}Pb$, $^{87}Sr/^{86}Sr$) and EM-II-like compositions, (medium $^{206}Pb/^{204}Pb$, low $^{143}Nd/^{144}Nd$, high $^{207}Pb/^{204}Pb$ $^{207}Pb/^{206}Pb$, $^{87}Sr/^{86}Sr$), which is generally considered to reflect the involvement of terrigenous sediments in mantle sources. Given the evolved nature of the RPV rocks (eight out of eleven samples having MgO <3 wt%) we believe that their isotope-isotope and isotope-SiO_2-MgO correlations reflect some degrees of interaction with local upper crust, represented by Hercynian granitoids, rather than mantle source contamination. The positive Nd-Hf and negative Sr-Hf isotopic correlation, as well as the positive Δ7/4 values and, to a minor extent, Δ8/4 (not shown), may be considered as further evidence for the involvement of a contaminating crustal component.

The UPV activity started during the last phases of the RPV activity (Fig. 3), but the two groups show completely different Sr-Nd-Pb-Os-Hf isotopic ratios. The Sr-Nd isotopic ratios of UPV point towards the EM-I end-member (Enriched Mantle Type I; Zindler and Hart, 1986; Lustrino and

Dallai, 2003; Hofmann, 2004). The most peculiar signature of the UPV rocks is their low $^{206}Pb/^{204}Pb$ and high $^{207}Pb/^{206}Pb$ and $^{208}Pb/^{206}Pb$ (Fig. 6b,c, 11). Despite that the Sr-Nd-Pb isotopic composition of the UPV rocks has been described in detail in several papers (Montanini et al., 1994; Gasperini et al., 2000; Lustrino et al., 2000, 2002, 2004, 2007a, 2007b; Fedele et al., 2007) a general consensus on the origin of these magmas has not yet been reached. In particular, two main models are proposed to explain the isotopic composition of these lavas: a) recycling of plume heads and b) complex styles of interaction between delaminated lower crust and ambient upper mantle.

The recycling of plume heads in the Sardinian mantle proposed by Gasperini et al. (2000) has been discussed in Lustrino et al., 2007a, 2011) and therefore it will not be repeated here. We simply note that "the storage of plume heads in the deep mantle through time" as requested by Gasperini et al. (2000) is unlikely from a geological point of view and hardly compatible with the composition and volume of the produced magma. More recently Bell et al (2013) explained the Sr-Nd-Pb isotopic compositions of the UPV rocks as the result of a lithospheric mantle fluxed by an alleged Late Triassic-Early Jurassic mantle plume responsible for the Neotethys Ocean opening. A totally different approach (Lustrino et al., 2000, 2002, 2007a; Lustrino, 2005; Peccerillo and Lustrino, 2005) invokes complex styles of interaction between lower crustal lithologies (eclogites to garnet-bearing pyroxenites) and ambient peridotitic upper mantle. Continental lower crust would undergo partial melting at upper mantle depths, releasing SiO_2-oversaturated melts (dacitic to rhyolitic in composition; e.g., Qian and Hermann, 2013) easily reacting with ambient upper mantle. The presence of lower crustal lithologies at upper mantle depths would be the consequence of delamination and detachment processes of the lower crust and uppermost lithospheric mantle related to density-induced gravitative contrast between dense lower crustal levels.

The distinct geochemical and isotopic characteristics of the UPV group can be briefly resumed as follows (Lustrino et al., 2007a): 1) relatively high SiO_2 (>45 wt%); 2) relatively low CaO (generally lower than 8.8 wt%); 3) relatively low CaO/Al_2O_3 (generally <0.58); 4) SiO_2-saturated to oversaturated (i.e., CIPW hypersthene- to quartz-normative) compositions; 5) relatively low High Field Strength Element (HFSE) and Heavy Rare Earth Element (HREE) contents; 6) moderately radiogenic $^{87}Sr/^{86}Sr$ composition (generally >0.7044); 7) low $^{143}Nd/^{144}Nd$ (<0.51264); 8) low $^{206}Pb/^{204}Pb$ (<18); 9) low $^{208}Pb/^{204}Pb$ (<38.2); 10) high $^{208}Pb/^{206}Pb$ (>2.10); 11) high $^{207}Pb/^{206}Pb$ (>0.86).

The peculiar geochemical signatures of the UPV rocks have been ascribed to an orthopyroxene-rich lithospheric mantle source (e.g., Lustrino et al., 2007a) originated from the contamination of SiO_2-rich melts with ambient peridotite. The acid melts would have derived from low degree partial melting of delaminated and detached ancient lower continental crust. During the gabbro-eclogite metamorphic change, the original lower crust assemblage would have experienced (Th,U)/Pb and Rb/Sr ratio decrease, while the Sm/Nd and Lu/Hf ratios remained virtually unchanged, due to their lesser vulnerability to metamorphic processes. Thus, the lower crust developed lower time-integrated $^{206}Pb/^{204}Pb$, $^{208}Pb/^{204}Pb$, $^{87}Sr/^{86}Sr$ (and higher $^{208}Pb/^{206}Pb$) ratios with respect to the upper continental crust. With aging, this material would have also developed lower $^{143}Nd/^{144}Nd$ and $^{176}Hf/^{177}Hf$ than typical upper crustal lithologies (see discussion in Liew et al., 1991; Lustrino, 2005, Willbold and Stracke 2006).

Oxygen isotope constraints

Most of the $\delta^{18}O$ values of the UPV rocks measured on mafic phases (olivine and clinopyroxene) are relatively low ($\delta^{18}O_{Ol}$ from +5.37 to +5.98 ‰, $\delta^{18}O_{Cpx}$ from +5.41 to +5.93 ‰; Table 1) and virtually undistinguishable from olivine and clinopyroxene of upper mantle ($\delta^{18}O_{Ol}$ = +5.2‰, $\delta^{18}O_{Cpx}$ = +5.5‰). Only one clinopyroxene from Capo Frasca shows slightly higher values ($\delta^{18}O_{Cpx}$ = +6.74 ‰; MAL32), but it crystallized from a relatively evolved magma (i.e., basaltic andesite; SiO_2 = 54.51 wt%, MgO = 6.26 wt%, Mg# = 0.56). The absence of mantle xenoliths (found in alkaline rocks only), coupled with the relatively evolved compositions, suggests the presence of shallow magma chamber at upper-middle crustal depths for the tholeiitic UPV melts. Here some interaction with country rocks during an AFC-type process, could have resulted in an increase of the $\delta^{18}O_{Cpx}$ and $^{87}Sr/^{86}Sr$, and a decrease in $^{143}Nd/^{144}Nd$, as actually observed (0.70495 and 0.51232, respectively; Table 1). A plagioclase sample from Gerrei (MGL23) is characterized by relatively high $\delta^{18}O_{Pl}$ value (+6.67 ‰), when compared to the average $\delta^{18}O_{Cpx}$ values.

Isotopic fractionation between olivine/clinopyroxene and basaltic melts is very low, if occurring at all (Eiler et al., 1997). Therefore, the $\delta^{18}O_{ol}$ and $\delta^{18}O_{cpx}$ values can be interpreted to reflect the correct oxygen isotopic composition of the melts from which they crystallized. In contrast, the isotopic fractionation between plagioclase and basaltic melts at high temperatures is not known exactly but it is thought to be limited ($\Delta^{18}O_{melt\text{-}plagioclase}$ ranging from -0.1 to -0.5 ‰; Baker et al.,

2000). Even when considering this uncertainty, the $\delta^{18}O$ whole-rock value of the Gerrei sample MGL23 remains higher than the rest of the UPV samples ($\delta^{18}O_{WR} \geq +6.17$ ‰). The sample has a relatively primitive character (i.e., SiO_2 = 49.28 wt%, MgO = 9.97 wt%, Mg# = 0.69, Ni = 248 ppm, Cr = 349 ppm; Table 1) and contains sporadic mantle xenoliths (Lustrino et al., 1996; 1999), both indicating rapid upwelling rates. These constraints are, therefore, compatible with limited stagnation time in crustal depth magma chambers. As consequence, the relatively high calculated $\delta^{18}O_{WR}$ values can be explained either with the presence of recycled crustal lithologies with high $\delta^{18}O$ values in the UPV mantle sources or with stronger than expected isotopic fractionation between plagioclase and the crystallizing melt. In the first case it should be noted that lower crustal lithologies have been invoked to explain the Sr-Nd-Pb isotopic features of the UPV magmas. However, such an interaction must have been very ancient, in order to retard the $^{206}Pb/^{204}Pb$ isotopic growth (see more detailed discussion in Lustrino, 2005 and Lustrino et al., 2007a). Given the known ionic diffusion velocities at mantle depths, any "exotic" $\delta^{18}O$ value deriving from crustal lithologies would have been buffered by the average $\delta^{18}O$ values of the ambient mantle in a relatively short time. Moreover, the crustal lithologies would be of lower continental origin, and therefore never experienced low temperature oxygen isotopic exchange able to change the original $^{18}O/^{16}O$ ratios.

In conclusion, the oxygen isotopic ratios of olivine and clinopyroxene in the most primitive UPV lavas show no evidence of interaction with typical upper crustal material. If lower continental crust has been involved or not in the genesis of the UPV rocks, this cannot be registered in the $\delta^{18}O_{Ol}$ and $\delta^{18}O_{Cpx}$ values because lower continental crust has oxygen isotopic compositions indistinguishable from those of upper mantle.

As concerns the RPV lavas, only two oxygen isotopic analyses are available, both from the porphyritic rocks of Capo Ferrato (CF and MAL3 samples; Table 1). The CF sample shows evolved composition (trachyte; SiO_2 = 61.43 wt%, MgO = 1.26 wt%, Mg# = 0.30). The measured $\delta^{18}O_{Pl}$ value (+7.17 ‰) is the highest among the Middle Miocene-Quaternary volcanic rocks of Sardinia and is coherent with the highest $^{87}Sr/^{86}Sr$ (0.70487) among the RPV group. We believe that the high $\delta^{18}O_{Pl}$ value could reflect some degree of interaction with local upper crust, rather than being the true expression of its mantle source. This conclusion is also supported by the relatively low $\delta^{18}O_{Ol}$

value measured in a less differentiated sample from the same district (MAL3; $\delta^{18}O_{Ol}$ = +5.43 ‰), assuming that the olivine crystallized before any contamination in a shallow magma chamber (e.g., by an AFC-like process). In conclusion, in agreement with the previous models based on trace elements and Sr-Nd-Pb-Hf isotopic ratios, RPV rocks are believed to represent the products of partial melting of mantle sources that experienced some interaction with upper crustal lithologies. The high $\delta^{18}O$ values of the trachytic sample CF is related to shallow level crustal contamination in shallow magma chambers.

Osmium isotope constraints

Most of the Earth's budget of Re and Os is stored in the core, the two elements being strongly siderophile. However, some important differences exist between Re and Os behaviour during upper mantle partial melting. Osmium is qualitatively considered to be a strongly compatible element in peridotitic assemblages, whereas Re is moderately incompatible (e.g., Shirey and Walker, 1998; Meisel et al., 2001; Hauri, 2002). As a consequence, mantle residua evolve with extremely low $^{187}Re/^{188}Os$ ratios (~0.1), leading unradiogenic $^{187}Os/^{188}Os$ isotopic ratios compared to the primitive upper mantle estimate. On the other hand, basaltic melts and crustal lithologies show much higher $^{187}Re/^{188}Os$ ratios ($^{187}Re/^{188}Os$ estimate of upper crust ~400; Esser and Turekian, 1993), therefore evolving to radiogenic $^{187}Os/^{188}Os$ (Hauri, 2002). Basaltic magmas (with low Os elemental content) passing through continental crust (with high to very high $^{187}Os/^{188}Os$, especially for ancient continental crusts, and high $^{187}Re/^{188}Os$) are, therefore, particularly sensitive to crustal contamination effects.

Only few Os isotopic data we have measured can be used because several analyses gave very radiogenic results. This is particularly true for the samples with the lowest Os abundance, being those more easily modifiable for $^{187}Os/^{188}Os$ as consequence of alteration or even very small degrees contamination *en-route* to the surface (Table 1). The supra-chondritic isotopic ratios and the $^{187}Os/^{188}Os$ vs. 1/Os linear trend observed for UPV rocks (R^2 = 0.92) are compatible with a magma mixing with a crustal component. This could reflect involvement of lower crustal material in the source of this rock group, in agreement with the results inferred from the oxygen isotope data the positive Δ7/4 and Δ8/4 values (Table 1). The Os isotopic variation is, however not supported by the constancy of the Sr isotopic ratios. It is possible to invoke the presence of a process that decouples

these two isotope systems, because of the different geochemical behaviour or Rb/Sr and Re/Os pairs. The relatively radiogenic Os isotopic ratios could be also related to a contribution by an old $^{187}Re/^{188}O$-rich pyroxenitic layer of lower-crustal origin, as already proposed on the basis of Pb isotopic ratios and several geochemical and petrological arguments (e.g., Lustrino et al., 2000, 2007a).

Simple mixing modelling between a potential crustal contaminant ($^{187}Os/^{188}Os$ = 0.710 and Os = 0.15 ppb; Component A of Jung et al., 2011) and a hypothetical pure mantle basaltic melt ($^{187}Os/^{188}Os$ = 0.120 and Os = 0.4 ppb; Jung et al., 2011) and between the same contaminant and a hypothetical mantle source ($^{187}Os/^{188}Os$ = 0.12542 and Os = 2 ppb) has been performed in order to constrain possible crustal contamination processes. $^{187}Os/^{188}Os$ values as high as 0.1579, recorded in sample MGV238, can be reached after the digestion up to 15% of a component A by a basaltic melt. If a much lower Os elemental content of the basaltic melt (down to 0.02 ppb; e.g., Dale et al., 2012) is assumed, the amount of recycled crust decreases to less than 1%. Choosing a more radiogenic crustal contaminant ($^{187}Os/^{188}Os$ = 1.004) with much lower elemental Os (0.0521 ppb; SD75 sample of Conticelli et al., 2007) and only slightly more crustal interaction (a few more percent mixing) would lead to very high isotopic ratios in the magmas (up to 25% of crustal component). These results clearly indicate the strong dependence of any mixing calculations from the input parameters.

The notably higher Os content of mantle peridotite require a much higher amount of recycled crustal material (component A) to increase the $^{187}Os/^{188}Os$ ratios up to values of sample MGV238 (~45%). Assuming a metasedimentary component like sample SD75, the amount of crustal interaction increases up to ~60%. These large amounts of crustal recycling (>40%) are geologically and geochemically highly improbable and for this reason we suggest that the Os isotopic signal is mostly related to magma contamination before arrival at the surface. The even more radiogenic $^{187}Os/^{188}Os$ ratios of two UPV samples (0.2945-0.4230) clearly reflect higher degrees of crustal contamination in magma chambers by mildly evolved Os-poor basaltic melts. Alternatively, preferential melting of radiogenic pyroxenites instead of peridotites derived from the underlying mantle, as suggested for the UPV magma source (see above), can explain the quite radiogenic composition of these young volcanic rocks (e.g., van Acken et al., 2010).

Towards a geological model for the SR rocks

The Late Eocene-Middle Miocene igneous activity in the Western Mediterranean has been classically related to the NW-directed subduction of oceanic lithosphere beneath the southern paleo-continental margin of Europe (see Lustrino et al., 2011 for a review). This generally accepted geological interpretation has been recently challenged by Carminati et al. (2012). On the basis of a detailed palinspastic reconstruction and several geological constraints, the authors strongly reduced the importance of a direct involvement of Alpine Tethys subduction to explain the first phases of the SR igneous activity in Sardinia. The beginning of the northwest-ward Apennine subduction has been placed around Late Eocene (~48-45 Ma; Lustrino et al., 2009; Carminati et al., 2010, 2012; Shimabukuro et al., 2012), whereas the bulk of the subduction-related igneous activity in Sardinia and neighbouring districts is much younger (~23-15 Ma; Lustrino et al., 2009, 2011; Réhault et al., 2012). In the time span between the beginning of Apennine subduction and the peak of the subduction-related magmatism in western Mediterranean, only discrete and limited igneous activities are recorded (northern Ligurian-Provençal Basin, ~43 Ma; south-eastern France, ~41 Ma; northwest Sardinia, ~38 Ma; southern Spain, ~38 Ma). The paucity of Eocene-Oligocene subduction-related igneous activity is not consistent with a continuous northwest-directed subduction model of the eastern branch of the Alpine Tethys (or the Mesogean Ocean). Why did the subduction-related igneous activity appear few Myr after the beginning of the Apennine subduction, then mostly disappeared for about 10-15 Myr and finally experienced a climax about 25 Myr after the beginning of subduction?

We propose that the earliest (~43-23 Ma) subduction-related igneous phases in the western Mediterranean are not directly related to the metamorphic dehydration processes of the subducting Alpine Tethys plate, but rather to the pushing effects of this plate over the ancient lower crust of the upper plate. Assuming a convergence rate between the upper (i.e., Europe) and lower plates (i.e., western branch of the Alpine Tethys) as slow as 1-3 cm/yr (e.g., Gueguen et al., 1998; Faccenna et al., 2001; Carminati et al., 2010, 2012) and a 45° angle of the subducting plate (Lustrino et al., 2009), the front of the Alpine Tethys slab would have reached the depth at which the amphibole is expected to breakdown (~80-120 km; Schmidt and Poli, 1998; Niida and Green, 1999; Syracuse and Abers, 2006) between 3.8 Myr (3 cm/yr, 80 km depth) and 17 Myr (1 cm/yr, 120 km depth) later. These values are compatible with a Late Eocene initiation of the Apennine subduction (~48-45 Ma)

as proposed by Lustrino et al. (2009). The main problem with this model, not addressed before, is represented by the horizontal distance of the volcanic arc from the subduction hinge. In classical palinspastic reconstructions (e.g., Rosenbaum et al., 2002; Lustrino et al., 2009, 2011, Carminati et al., 2010, 2012; Molli and Malavieille, 2011; Shimubukuro et al., 2012) the upper plate of the Apennine subduction system was represented, from the most external to the most internal zones, by the present-day Provence, the Sardinia-Corsica block and Calabria-Peloritani Mts. Terrane (Fig. 2). Assuming a 45° dipping of the Alpine Tethys plate, the depths of 80-120 km are reached at the same horizontal distance from the subduction hinge (80-120 km). Assuming a steeper subduction dip (~65°), typical of west-directed subductions (Doglioni et al. 1999, 2007), the horizontal distance from the hinge is strongly reduced to 37 and 56 km. In other words, the volcanic arc should be expected at a horizontal distance from the trench in a range of ~37 to ~120 km. Conversely, following the palinspastic reconstruction of Carminati et al. (2012), the horizontal distance from the Apennine subduction hinge and the volcanic arc is 200 to 400 km in the time range 42-38 Ma (Fig. 2). Such a horizontal distance from the hinge and the depth of amphibole breakdown can be reached only assuming improbably shallow subduction, with inclination of the slab in the order of 10-20°, never recorded in west-directed subductions (Riguzzi et al., 2010).

In summary, a single oceanic plate subducting beneath a continental plate can explain the chemical and isotopic composition of SR rocks of Sardinia and the other volcanic rocks with subduction-related geochemical signature of the western Mediterranean, but not their areal distribution. Whatever subduction dip, convergence rate and depth of partial melting is chosen, it is not possible to obtain a geologically sound model able to explain the spatial-temporal relationships of the western Mediterranean subduction-related igneous districts. Unfortunately the geochemical and isotopic coverage of samples older than 23-25 Ma is very poor, mostly because their burial beneath the thick Early Miocene pyroclastic successions.

In this context, the composition of the Calabona microdiorite (~38 Ma) can be used to constrain possible chemical variation with age within the SR rock group. The evolved composition of this sample (SiO_2 = 63 wt%; MgO = 2.51 wt%), however, strongly reduces its usefulness for comparing major and incompatible trace element compositions with the bulk of the (less evolved) SR Sardinian rocks (~23-15 Ma). Nevertheless, the Calabona microdiorite shows the lowest $^{206}Pb/^{204}Pb$ (18.41) and one of the lowest $^{143}Nd/^{144}Nd$ isotopic ratios (0.512252) among the SR rock group. These

isotopic ratios are compatible with a presence of (recycled) lower crustal lithologies in the Calabona magma source, therefore reinforcing the hypothesis that the earliest manifestations of the SR magmatism are related to partial melting of Hercynian lower crust rather than to the dehydration processes of Alpine Tethys or Mesogean oceanic crust.

Open questions for future studies

Below are listed some general questions only partially addressed by this study and that should deserve more attention in order to produce a geologically-grounded petrogenetic model for the Western Mediterranean evolution.

1) *What is the origin of CaO-rich SR rocks?* All the SR rocks and particularly the least evolved compositions are characterized by an anomalously CaO-rich composition compared with the UPV and RPV rocks (Fig. 12). This feature is mirrored by other western Mediterranean igneous districts (e.g., Spain and Maghreb) where "subduction-related" and "intraplate-like" volcanic rocks are present (Lustrino et al., 2011, and references therein). The CaO-rich composition of the SR primitive melts is seemingly in contrast with a depleted DMM-like source evidenced from the Sr-Nd isotopic point of view and the low $(La/Lu)_N$ ratios (~4.2-1.4). It is worth noting that ultracalcic primitive magma compositions have been widely documented (both as whole-rock compositions and as melt inclusions) in several tectonic settings. Their genesis has been alternatively ascribed to: 1) interaction of a picritic melt with a clinopyroxene-rich source; 2) melting of a websteritic/wehrlitic source; 3) melting of carbonated or (CO_2+H_2O)-fluxed lherzolite/harzburgite; 4) melting of an almost refractory lherzolite at high temperatures and low pressures (e.g., Kamenetsky et al., 1998; Schiano et al., 2000; Schwab and Johnson, 2001; Médard et al., 2004 and references therein). More specifically, the origin of hypersthene-normative ultracalcic melts has been related either to a high-T shallow-P melting (> 1350 °C at ~1 GPa) of a wehrlitic mantle source or to low-T melting of an almost refractory clinopyroxene-poor lherzolite (or harzburgite; Médard et al., 2004). If a moderate volatile content is assumed, the unrealistically high T values proposed by Médard et al (2004) can be sensitively lowered and the above processes become quite likely for the genesis of SR rocks. The least evolved SR rocks of Sardinia do not reach the MgO- and CaO-rich compositions of the typical hy-normative ultracalcic primitive melts (i.e., Mg# >60; CaO >13.5 wt%; CaO/Al_2O_3 >1), possibly suggesting that they experienced some crystal fractionation. This is also consistent with the lower

Mg# values of their olivine and clinopyroxene crystals ($Mg\#_{ol}$ = 0.73-0.87, $Mg\#_{cpx}$ = 0.66-0.84; Morra et al., 1997) compared with those of the liquidus phases for the experimentally investigated ultracalcic melts (0.90-0.91 and 0.92-0.93, respectively). Alternatively, the SR basalts can be considered as the product of a mixture between ultracalcic and basaltic melts (see Schiano et al., 2000) or the products of partial melting of a more Fe-rich source (a feature compatible with a clinopyroxene-rich arc cumulate).

A completely specular approach is considering the "anorogenic" products as being anomalously CaO-poor compared with SR rock compositions. In particular, the low CaO content of the UPV rocks has been already pointed out by Lustrino et al. (2007a) and tentatively related to the existence of orthopyroxene-rich metasomes in their source region. These pyroxene-rich layers could be related to the interaction of lower crust-derived silica oversaturated melts interacting with mantle olivine. Another cause responsible for the relatively low CaO content of the "anorogenic" Sardinian rocks could be a process similar to that proposed by Zeng et al. (2013) for the mantle xenolith-rich Nanjing basalts in Eastern China. These authors propose that the incongruent melting of mantle diopside produces CaO-poor melts plus a CaO-rich spongy clinopyroxene residuum. The interaction of these partial melts with host magma can explain the anomalously low CaO content of the Chinese basalts. The common presence of mantle xenoliths in the alkaline basaltic rocks of Sardinia, coupled with the common presence of spongy-textured diopside in the xenoliths (Lustrino et al., 1999; Rocco et al., 2012) could favour also this hypothesis to explain the differences in CaO content between these and the SR rocks.

2) *What is the significance of peralkaline magmatism in a subduction-related setting?* Peralkaline magmatic activity is commonly associated to oceanic intraplate settings (e.g., Azores, N Atlantic; Mungall and Martin, 1995) or continental rift settings (e.g., East Africa, NW Libya, Morocco, Sicily Channel; Avanzinelli et al., 2004; Civetta et al., 1998; Berger et al., 2009; Ronga et al., 2010; Lustrino et al., 2012; White et al., 2012). In the Sulcis area, however, peralkaline rhyolites (found in the comendite type-locality) are genetically associated with subduction-related rocks as in few other cases worldwide (e.g., New Zealand, Papua New Guinea and southern Mongolia; Smith et al., 1977; Kovalenko et al., 2009; 2010). Moreover, clinopyroxene and amphibole crystals in Sulcis comendites show melt inclusions resembling the composition of the closely associated (both in time and space) Isola del Toro trachytes (Fig. 1). On these grounds Ronga (2011) proposed for the Sulcis peralkaline

volcanic rocks an origin after a mixing between the Sulcis metaluminous rhyolites and Capo Ferrato-like trachytes in a 40:60 to 50:50 ratio.

3) *What is the origin of the RPV activity?* The origin of the RPV activity is not completely understood. Geochemical and petrological constraints suggest a derivation from mantle sources not directly modified by subduction-related metasomatic processes. This is quite surprising, considering that the previous igneous activity, ended about 3 Myr earlier the beginning of RPV, shows clear subduction-related geochemical characteristics. Such an abrupt change in elemental and isotopic composition can be explained only with the activation of different mantle sources, possibly placed in the shallowest lithospheric mantle for the SR rocks and in slightly deeper "asthenospheric" sources for the RPV. The origin of the oldest RPV rocks is related to the beginning of continental stretching in the embryonic Tyrrhenian Sea, with the first stages of crustal separation between Sardinia and Corsica-Peloritani block (Lustrino et al., 2007b; Carminati et al., 2010, 2012). Interestingly, the RPV activity is part of a larger volcanic area characterized by normal faults and punctual sodic alkaline magmatism running from NW Libya to southern Sardinia (e.g., Lustrino et al., 2012 and references therein).

4) *Why the RPV activity is concentrated in southern Sardinia only?* One possibility is that the youngest UPV products covered previous RPV outcrops. Alternatively, the existence of different mantle sources in southern and central-northern Sardinia could be invoked. This hypothesis is geologically sounded because the island is, the result of a collage of different continental terranes collided during different Paleozoic (or even older) orogenies.

5) *Why do the RPV and UPV show such different isotopic composition?* The most likely origin of the RPV igneous activity is partial melting associated with passive adiabatic upwelling of a sub-lithospheric mantle, after the supra-subduction mantle wedge had been purged by the previous slab-derived modifications. The engine responsible for the UPV phase is not yet clear. During Plio-Pleistocene times the hinge of the Apennine oceanic subduction had moved some hundreds km towards SE, associated with abundant subduction-related igneous activity along the western Tyrrhenian coast (Tuscan, Roman and Neapolitan igneous provinces) and in SE Tyrrhenian Sea (Aeolian Islands). The development of the Campidano Graben in southern Sardinia testifies the presence of extensional movements that have been traced towards SE down to the Sicily Channel (e.g., Corti et al., 2006) and northern Libya (e.g., Capitanio et al., 2011), also with abundant

production of sodic alkaline melts (e.g., Lustrino and Wilson, 2007; Lustrino et al., 2012). As previously proposed, it is possible that the southern Sardinia belongs to structurally and chemically different domains compared with the central-northern sectors. These two terranes may have been accreted during Early Paleozoic or Proterozoic times. The following diffuse Late Paleozoic Hercynian Orogeny may have obscured all or most of the traces of previous orogeneses.

6) *Did the lower crust delamination and detachment occur along with the stretching of the over-thickened crust during the Ligurian-Provençal and the Tyrrhenian Basin formation?* A strong density increase is recorded during the gabbro-eclogite transformation developed during continent-continent collisional phases. Continent-continent collision has been recorded at least two times during Paleozoic times (Ordovician and Carboniferous-Permian) and likely also before. If the lower continental crust would have delaminated and detached only few tens Myr before the igneous activity, the $^{238}U/^{204}Pb$ decrease would have not evolved to low $^{206}Pb/^{204}Pb$ ratios. In order to produce low $^{206}Pb/^{204}Pb$, the $^{238}U/^{204}Pb$ system must have been shut down (to values close to 0) in the order of 1-2 Ga. This means that the processes responsible for the $^{238}U/^{204}Pb$ decrease are likely related to Proterozoic tectonics, an eon very poorly constrained for this region of the Earth.

7) *Why is the Plio-Quaternary circum-Tyrrhenian volcanism so different on the eastern and the western shoulder?* The Tyrrhenian Sea grew mostly from Late Miocene (~12-10 Ma) to Present. During its formation, the igneous activity along the western and eastern borders shifted continuously to E-SE (Carminati et al., 2012, and references therein). During this slab retreat, an abundant subduction-related igneous activity developed from the Tuscan district towards peninsular Italy (Roman and Neapolitan potassic to ultrapotassic magmatism) and to the Aeolian islands, possibly also including the activity associated with the stretching of the Tyrrhenian Sea (Trua et al., 2007; Lustrino et al., 2011, and references therein). Such magmatism is therefore a consequence of the metasomatism related to the fluids released from the downgoing Calabrian slab. On the other hand, the mildly sodic alkaline to tholeiitic magmatism on the western border of the Tyrrhenian was far away from the subduction front, acquiring the so called “anorogenic” geochemical signature.

Acknowledgements

This paper is dedicated to the memory of John J. Mahoney, prematurely passed away in November 2012. JJ was a precious teacher and colleague for many of us. Thanks to Sandro Conticelli (Florence,

Italy) for the help in analyzing the Sr-Nd isotopic ratios of some SR samples and to Luigi Dallai for the oxygen isotope analyses. The manuscript benefitted of the thorough review of Chris Dale (Durham, UK) and an anonymous reviewer plus the editorial handling of Dejan Prelevic (Mainz, Germany). ML thanks, as usual, Enrica, Bianca and Laura for their immense patience during the writing of this manuscript. Research grants to ML from PRIN (2008HMHYFP_005 and 20107ESMX9_001) and Ricerche Ateneo (2010, 2011, 2012) are warmly acknowledged. ML thanks Roger Waters, David Gilmour, Nick Mason and the late Rick Wright and Syd Barret for being properly lunatic for a long period of their life.

ANALYTICAL TECHNIQUES

Major and Trace elements

Clean rock chips of each sample were obtained using a steel jaw crusher. These were washed in distilled water, dried out and pulverized in a low-blank agate mortar. Major elements were analyzed in Naples using a Philips PW1400 X-Ray fluorescence spectrometer (XRF), following the procedure described by Melluso et al. (2005). Analytical precision is estimated to be within 1% for SiO_2, TiO_2, Al_2O_3, Fe_2O_3 and CaO, and better than 6% for K_2O, ± 0.03 wt% for MnO and P_2O_5. Na and Mg were analyzed by atomic absorption spectrometry, with precision better than 2%. L.O.I. (weight loss on ignition) was determined gravimetrically. Trace elements were analyzed by inductively coupled plasma-mass spectrometry (ICP-MS) at C.R.P.G. Nancy (France) and Actlabs (Ontario, Canada), with typical precision <5%. Samples are mixed with a flux of lithium metaborate and lithium tetraborate and fused in an induction furnace. The fusion process ensures total metals, particularly for elements like REE, in resistate phases. The molten melt is immediately poured into a solution of 5% nitric acid containing an internal standard, and mixed continuously until completely dissolved (~30 minutes). The sample solution is spiked with internal standards to cover the entire mass range, and is further diluted to cover the entire mass range, is further diluted and is introduced into a Perkin Elmer SCIEX ELAN 6000 or 6100 ICP-MS using a proprietary sample introduction methodology. Further information on ICP-MS can be found in www.actlabs.com and www.crpg.cnrs-nancy.fr .

Sr-Nd-Pb-O-Hf-Os isotopes

Strontium and Nd isotope ratios were measured in a static mode on a multiple collectors Triton-Ti® mass spectrometer at the Dipartimento di Scienze della Terra of the University of Florence (Italy) according to the method described in Avanzinelli et al. (2005). The design of the Triton-Ti® allow the rotation of the amplifiers (Virtual Amplifier) among the different cups thus the electronic bias is cancelled out. The Virtual Amplifier permits the achievement of good internal precision even during static measurements with significant time saving (40 minutes each analysis). Five collectors were used for Sr and eight for Nd. Mass fractionation effects were normalized, using an exponential law, to $^{86}Sr/^{88}Sr = 0.1194$ and $^{146}Nd/^{144}Nd=0.7219$, respectively. All errors reported for within run precision are 2σ (2 standard error). Repeated analyses of SRM 987 and La Jolla standards yielded values of $^{87}Sr/^{86}Sr = 0.710269 \pm 8$ (n = 17), and $^{143}Nd/^{144}Nd = 0.511844 \pm 7$ (n = 20), respectively. Total process blank measured for Sr was 40 pg. Blank correction was therefore negligible relative to the 130 μg of Sr analyzed for the samples.

Lead isotope ratios were measured with a VG Sector at the School of Ocean and Earth Science Technology (SOEST), University of Hawaii at Manoa (USA) following the procedure described in Peng and Mahoney (1995). Twenty-three lead ratios were misured with a FINNIGAN MAT 262 thermal ionization mass spectrometer at U.S. Geological Survey (Reston-Virginia), following the analytical techniques described in Ayuso et al. (2009) and references therein. Data are normalized relative to reported values of $^{87}Sr/^{86}Sr = 0.71024$ for NBS 987 Sr, $^{143}Nd/^{144}Nd = 0.511845$ for La Jolla Nd, and Pb isotope values of Todt et al. (1996) for NBS 981 Pb. The total range measured for NBS 981 Pb it was ± 0.011 for $^{206}Pb/^{204}Pb$, ± 0.010 for $^{207}Pb/^{204}Pb$, and ± 0.031 for $^{208}Pb/^{204}Pb$. Within-run errors on the isotopic data above are less than or equal to the external uncertainties on these standards. Total procedural blanks are negligible.

Oxygen isotopes

Oxygen isotope data on mineral separates were measured by conventional laser fluorination (Sharp, 1995) at the CNR-Istituto di Geologia Ambientale e Geoingegneria in Rome, Italy. A 15 W CO_2 laser, operating at a wavelength of 10.6 μm, was employed to irradiate the samples and pure F_2 desorbed at 320 °C from K_3NiF_7 salt (Asprey, 1976) was used to react ~2 mg of clinopyroxene, olivine and plagioclase fragments placed in a 3 mm diameter hole, within a 32-hole nickel sample plug. The O_2 produced was purified of excess fluorine by a KBr trap at 160 °C and of trace NFx by-products of laser fluorination using a 13 Å zeolite molecular sieve and liquid nitrogen-ethanol mixture (Clayton and Mayeda, 1983). The gas was then introduced into a Finnigan delta plus mass spectrometer and analyzed for oxygen isotope composition, and mineral yields were controlled to be quantitative by an empirical regression curve based on samples with known $\delta^{18}O$ versus PO_2 values in the MS bellow. During each set of analyses, two to four aliquots of laboratory quartz standards were measured with an average reproducibility of <± 0.10‰ (1r) and no data correction was adopted. A total of 8 LAUS1 ($\delta^{18}O$ = 18.15‰) and 10 QMS ($\delta^{18}O$ = 14.05‰) standard samples were measured during the time of this study, with an average $\delta^{18}O$ value of 18.21 ± 0.10‰ and 13.98 ± 0.15‰ (2r), respectively. All the results are reported in the standard per mil notation and the $\delta^{18}O$ values are relative to SMOW. At least two fragments were analyzed for each mineral and variation within the same sample is less than the precision of standards.

Hafnium isotopes

For Hf-isotope analyses whole rock powders were flux fused with Li-metaborate and dissolved in 2 mol/l HCl, followed by cation exchange and extraction chromatographic separation at the Geological Institute of the University of Copenhagen, as described in the literature (Ulfbeck et al., 2003). Hafnium isotope analyses were carried out at GEOMAR using an AXIOM MC-ICP-MS (multiple collector inductively coupled plasma mass spectrometer) as described in detail in Geldmacher et al. (2006). The measured Hf-isotope data were drift corrected by standard bracketing (four samples bracketed by JMC475) and normalized to a JMC475 value of 0.282163 (Nowell et al., 1998). Measurements of JMC475 during the analysis of present samples yielded a mean value of 0.282144 ± 8 (2σ.; n = 8).

Os isotopes

For the measurements of the Os isotopic composition two grams of sample powder were digested in a high pressure asher (HPA-S, Anton Paar, Austria) and separated from rhenium through distillation into concentrated HBr and a subsequent microdistillation (for more details see Reisberg and Meisel, 2002 and Meisel et al. 2001). The Os isotopic ratios were determined by negative thermal ion mass spectrometry (N-TIMS) on a Finnigan MAT262 at the CRPG/CNRS Nancy, France. by using the methods of Creaser et al. (1991) and Walczyk et al (1991), normalized to a $^{192}Os/^{188}Os$ of 3.0827 (Nier, 1937). Total procedure blanks were 1 pg for Re and Os in average and thus negligible. Spike and oxide interferences were corrected separately in a spreadsheet.

REFERENCES

Alvarez, W., 1974. Fragmentation of the Alpine orogenic belt by microplate dispersal. Nature, 248, 309-314.

Arculus, R.J., 2003. Use and abuse of the terms calcalkaline and calcalkalic. Journal of Petrology 44, 929-935.

Ayuso, R.A., Haeussler, P.J., Bradley, D.C., Farris, D.W., Foley, N.K., Wandless, G.A., 2009. The role of ridge subduction in determining the geochemistry and Nd-Sr-Pb isotopic evolution of the Kodiak batholit in southern Alaska. Tectonophysics 464, 137-163.

Asprey, L.B., 1976. The preparation of very pure F_2 gas. Journal of Fluorine Chemistry 7, 359-361.

Avanzinelli, R., Bindi, L., Menchetti, S., Conticelli, S., 2004. Crystallization and genesis of peralkaline magmas from Pantelleria volcano, Italy: an integrated petrological and crystal-chemical study. Lithos 73, 41-69.

Avanzinelli, R., Boari, E., Conticelli, S., Francalanci, L., Guarnieri, L., Perini, G., Petrone, C.M., Tommasini, S., Ulivi, M., 2005. High precision Sr, Nd and Pb isotopic analyses and reproducibility using new generation thermal ionisation mass spectrometer: aims and prespective for isotope geology applications. Periodico di Mineralogia 74, 147-166.

Avanzinelli, R., Lustrino, M., Mattei, M., Melluso, L., Conticelli, S., 2009. Potassic and ultrapotassic magmatism in the circum-Tyrrhenian region: significance of carbonated pelitic vs. pelitic sediment recycling at destructive plate margins. Lithos 113, 213-227.

Baker, J.A., MacPherson, C.G., Menzies, M.A., Thirlwall, M.F., Al-Kadasi, M., Mattey, P., 2000. Resolving crustal and mantle contributions to continental flood volcanism, Yemen; constraints from mineral oxygen isotope data. Journal of Petrology 41, 1805-1820.

Beccaluva, L., Bianchini, G., Mameli, P., Natali, C., in press. Miocene shoshonite volcanism in Sardinia: implications for magma sources and geodynamic evolution of the central-western Mediterranean. Lithos, this volume.

Beccaluva, L., Brotzu, P., Macciotta, G., Morbidelli, L., Serri, G., Traversa, G., 1989. Cainozoic tectono-magmatic evolution and inferred mantle sources in the Sardo-Tyrrhenian area, in: Boriani, A., Bonafede, M., Piccardo, G.B., Vai, G.B. (Eds.), Lithosphere in Italy. Accademia Nazionale dei Lincei, Roma, pp. 229-248.

Beccaluva, L., Civetta, L., Macciotta, G., Ricci, C.A., 1985. Geochronology in Sardinia: results and problems. Rendiconti della Società Italiana di Mineralogia e Petrologia 40, 57-72.

Bell, K., Lavecchia, G., Rosatelli, G., 2013. Cenozoic Italian magmatism – isotope constraints for possible plume-related activity. Journal of South American Earth Sciences 41, 22-40.

Berger, J., Ennih, N., Mercier, J.-C.C., Liégeois, J.-P., Demaiffe, D., 2009. The role of fractional crystallization and late-stage peralkaline melt segregation in the mineralogical evolution of Cenozoic nephelinites/phonolites from Saghro (SE Morocco). Mineralogical Magazine 73, 59-82.

Bolhar, R., Kamber, B.S., Collerson, K.D., 2007. U-Th-Pb fractionation in Archaean lower continental crust: implications for terrestrial Pb isotope systematics. Earth and Planetary Science Letters 254, 127-145.

Blusztajn, J., Hegner, E., 2002. Osmium isotopic systematics of melilitites from the Tertiary Central European Volcanic Province in SW Germany. Chemical Geology 189, 91-103.

Brotzu, P., Callegari, E., Morra, V., Ruffini, R., 1997a. The orogenic basalt-andesite suites from the Tertiary volcanic complex of Narcao, S-W Sardinia (Italy): petrology, geochemistry and Sr-isotope characteristics. Periodico di Mineralogia 66, 101-150.

Brotzu, P., Lonis, R., Melluso, L., Morbidelli, L., Traversa, G., Franciosi, L., 1997b. Petrology and evolution of calcalkaline magmas from the Arcuentu volcanic complex (SW Sardinia, Italy). Periodico di Mineralogia 66, 151-184.

Capitanio, F.A., Faccenna, C., Funiciello, R., Salvini, F., 2011. Recent tectonics of Tripolitania, Libya: and intraplate record of Mediterranean subduction. Geological Society of London Special Publication 357, 319-328.

Carminati, E., Lustrino, M., Cuffaro, M., Doglioni, C., 2010. Tectonics, magmatism and geodynamics of Italy: what we know and what we imagine. Journal of the Virtual Explorer 36, paper 9. doi:10.3809/jvirtex.2010.00226.

Carminati, E., Lustrino, M., Doglioni, C., 2012. Geodynamic evolution of the central and western Mediterranean: Tectonic vs. Igneous constraints. Tectonophysics 579, 173-192.

Cherchi, A., Mancin, N., Montadert, L., Murru, M., Putzu, M.T., Schiavinotto, F., Verrubbi, V., 2008. The stratigraphic response to the Oligo-Miocene extension in the western Mediterranean from observations on the Sardinia graben system (Italy). Bulletin de la Societe Geologique de France 179, 267-287.

Chiba, H., Chacko, T., Clayton, R.N., Goldsmith, J.R., 1989. Oxygen isotopic fractionation involving diopside, magnetite and calcite: application to geothermometry. Geochimica et Cosmochimica Acta 53, 2985-2995.

Cioni, R., Clocchiatti, R., Di Paola, G.M., Santacroce, R., Tonarini, S., 1982. Miocene calc-alkaline heritage in the Pliocene post-collisional volcanism of Monte Arci (Sardinia, Italy). Journal of Volcanology and Geothermal Research 14, 133-167.

Civetta, L., D'Antonio, M, Orsi, G., Tilton, G.R., 1998. The geochemistry of volcanic rocks from Pantelleria island, Sicily Channel: petrogenesis and characteristics of the mantle source region. Journal of Petrology 39, 1453-1491.

Clayton, R.N., Mayeda, T.K., 1983. Oxygen isotopes in eucrites, shergottites, nakhilites, and chassignites. Earth and Planetary Science Letters 62, 1-6.

Cohen, R.S., O'Nions, R.K., Dawson, J.B., 1984. Isotope geochemistry of xenoliths from East Africa: implications for development of mantle reservoirs and their interaction. Earth and Planetary Science Letters 68, 209-220.

Conte, A.M., 1997. Petrology and geochemistry of Tertiary calc-alkaline magmatic rocks from the Sarroch domain (Sardinia, Italy). Periodico di Mineralogia 66, 63-100.

Conte, A.M., Palladino, D.M., Perinelli, C., Argenti, E., 2010. Petrogenesis of the High-Alumina basalt–andesite suite from Sant'Antioco Island, SW Sardinia, Italy. Periodico di Mineralogia 79, 27-55.

Conticelli, S., Carlson, R.W., Widom, E., Serri, G., 2007. Chemical and isotopic composition (Os, Pb, Nd, and Sr) of Neogene to Quaternary calc-alkalic, shoshonitic, and ultrapotassic mafic rocks from the Italian peninsula: Inferences on the nature of their mantle sources, in: Beccaluva, L., Bianchini, G., Wilson, M. (Eds.), Cenozoic Volcanism in the Mediterranean Area. Geological Society of America Special Paper 418, 171-202.

Corti, G., Cuffaro, M., Doglioni, C., Innocenti, F., Manetti, P., 2006. Coexisting geodynamic processes in the Sicily Channel, in: Dilek, Y., Pavlides, S. (Eds.), Tectonics and magmatism in the Mediterranean region and Asia. Geological Society of America Special Paper 409, 83-96.

Coulon, C., 1977. Le volcanisme calco-alcaline cénozoique de Sardaigne (Italie): petrography, géochimie et genèse des laves andesitiques et des ignimbrites. Signification geodinamique. Thèse, Université Marseille, 385 pp.

Creaser, R.A., Papanastassiou, D.A., Wassenburg, G.J., 1991. Negative thermal ion mass spectrometry of osmium, rhenium and iridium. Geochimica et Cosmochimica Acta 55, 397-401.

Doglioni, C., Carminati, E., Cuffaro, M., Scrocca, D., 2007. Subduction kinematics and dynamic constraints. Earth-Science Reviews 83, 125-175.

Doglioni, C., Gueguen, E., Harabaglia, P., Mongelli, F., 1999. On the origin of west-directed subduction zones and applications to the western Mediterranean, in: Durand, B., Jolivet, L., Horvath, F., Seranne, M. (Eds.), The Mediterranean basins: Tertiary extension within the Alpine orogen. Geological Society of London 156, pp. 541-561.

Downes, H., Thirlwall, M.F., Trayhorn, S.C., 2001. Miocene subduction-related magmatism in Sardinia: Sr-Nd and oxygen isotopic evidence for mantle source enrichment. Journal of Volcanology and Geothermal Research 106, 1-21.

Duggen, S., Hoernle, K., van den Bogaard, P., Garbe-Schonberg, D., 2005. Post-collisional transition from subduction- to intraplate-type magmatism in the westernmost Mediterranean: evidence for continental-edge delamination of subcontinental lithosphere. Journal of Petrology 46, 1155-1201.

Duggen, S., Hoernle, K., Klugel, A., Geldmacher, J., Thirlwall, M., Hauff, F., Lowry, D., Oates, N., 2008. Geochemical zonation of the Miocene Alboran Basin volcanism (westernmost Mediterranean): geodynamic implications. Contributions to Mineralogy and Petrology 156, 577-593.

Duncan, R., Ginesu, S., Secchi, F., Sias, F., 2011. The recent evolution of the Sinis region (western coast of Sardinia, Italy) on the basis of new radiometric data of the Pliocenic volcanism. Geografia Fisica e Dinamica Quaternaria, 34, 175-181.

Eiler, J.M., Farley, K.A., Walley, J.W., Hauri, E., Craig, H., Hart, S.R., Stolper, E.M., 1997. Oxygen isotope variations in ocean island basalt phenocrysts. Geochimica et Cosmochimica Acta 61, 2281-2293.

Esser, B.K., Turekian, K.K., 1993. The osmium isotopic composition of the continental crust. Geochimica et Cosmochimica Acta 57, 3093-3104.

Faccenna, C., Becker, T.W., Lucente, F.P., Jolivet, L., Rossetti, F., 2001. History of subduction and back-arc extension in the central Mediterranean. Geophysical Journal International 145, 809-820.

Faccenna, C., Speranza, F., D'Ajello Caracciolo, F., Mattei, M., Oggiano, G., 2002. Extensional tectonics on Sardinia (Italy): insights into the arc-back-arc transitional regime. Tectonophysics, 356, 213-232.

Fedele, L., Lustrino, M., Melluso, L., Morra, V., d'Amelio, F., 2007. The Pliocene Montiferro volcanic complex (central-western Sardinia, Italy): Geochemical observations and petrological implications. Periodico di Mineralogia 76, 101-136.

Franciosi, L., Lustrino, M., Melluso, L., Morra, V., D'Antonio, M., 2003. Geochemical characteristics and mantle sources of the Oligo-Miocene primitive basalts from Sardinia: the role of subduction components. Ofioliti 28, 105-114.

Gasperini, D., Blichert-Toft, J., Bosch, D., Del Moro, A., Macera, P., Albarède, F., 2002, Upwelling of deep mantle material through a plate window: Evidence from the geochemistry of Italian basaltic volcanics. Journal of Geophysical Research 107, doi:10.1029/2001JB000418

Gasperini, D., Blichert-Toft, J., Bosch, D., Del Moro, A., Macera, P., Télouk, P., Albarède, F., 2000. Evidence from Sardinian basalt geochemistry for recycling of plume heads into the Earth's mantle. Nature 408, 701-704.

Gattacceca, J., Deino, A., Rizzo, R., Jones, D.S., Henry, B., Beaudoin, B., Vedeboin, F., 2007. Miocene rotation of Sardinia: new paleomagnetic and geochronological constraints and geodynamic implications. Earth and Planetary Science Letters 258, 359-377.

Geldmacher, J., Hoernle, K., Klügel, A., v.d. Bogaard, P., Wombacher, F., Berning, B. 2006. Origin and geochemical evolution of the Madeira-Tore Rise (eastern North Atlantic). Journal of Geophysical Research 111, B09206, doi:10.1029/2005JB003931

Guarino, V., Fedele, L., Franciosi, L., Lonis, R., Lustrino, M., Marrazzo, M., Melluso, L., Morra, V., Rocco, I., Ronga, F., 2011. Mineral compositions and magmatic evolution of the calcalkaline rocks of northwestern Sardinia, Italy. Periodico di Mineralogia 80, 517-545.

Gueguen, E., Doglioni, C., Fernandez, M., 1998. On the post-25 Ma geodynamic evolution of the western Mediterranean. Tectonophysics 298, 259-269.

Halliday, A.N., Dickin, A.P., Hunter, R.N., Davies, G.R., Dempster, T.J., Hamilton, P.J., Upton, B.G.J., 1993. Formation and composition of the lower continental crust: evidence from Scottish xenolith suites. JOurnal of Geophysical Research 98, 581-607.

Harangi, S.Z., Downes, H., Seghedi, I., 2006. Tertiary-Quaternary subduction processes and related magmatism in the Alpine-Mediterranean region, in: Gee, D., Stephenson, R. (Eds.), European Lithosphere Dynamics. Geological Society of London Memoirs 32, pp. 167-190.

Hauri, E.K., 2002. Osmium isotopes and mantle convection. Philosophical Transactions of the Royal Society of London 360, 2371-2382.

Hofmann, A.W., 2004. Sampling mantle heterogeneity trough oceanic basalts: isotopes and trace elements, in: Carlson, R.W. (Ed.), Treatise on Geochemistry, The Mantle and Core 2, 61-101.

Jung, S., Pfander, J.A., Brauns, M., Maas, R., 2011. Crustal contamination and mantle source characteristics in continental intra-plate volcanic rocks: Pb, Hf and Os isotopes from central European volcanic province basalts. Geochimica et Cosmochimica Acta 75, 2664-2683.

Jung, S., Pfander, J.A., Brugmann, G., Stracke, A., 2005. Sources of primitive alkaline volcanic rocks from the Central European Volcanic Province (Rhon, Germany) inferred from Hf, Os and Pb isotopes. Contributions to Mineralogy and Petrology 150, 546-559.

Kamenetsky, V.S., Eggins, S.M., Crawford, A.J., Green, D.H., Gasparon, M., Falloon, T.J., 1998. Calcic melt inclusions in primitive olivine at 43°N MAR: evidence for melt-rock reaction/melting involving clinopyroxene-rich lithologies during MORB generation. Earth and Planetary Science Letters 160, 115-132.

Kempton, P.D., Harmon, R.S., Hawkesworth, C.J., Moorbath, S., 1990. Petrology and geochemistry of lower crustal granulites from the Geronimo volcanic field, southeastern Arizona. Geochimica et Cosmochimica Acta 54, 3401-3426.

Kim, T., Nakai, S., Gasperini, D., 2011. Lithium abundance and isotope composition of Logudoro basalts, Sardinia: origin of light Li signature. Geochemical Journal 45, 323-340.

Kovalenko, V.I., Naumov, V.B., Girnis, A.V., Dorofeeva, V.A., Yarmolyuk, V.V., 2009. Peralkaline silicic melts of island arcs, active continental margins and intraplate continental settings: evidence from the investigation of melt inclusions in minerals and quenched glasses of rocks. Petrology 17, 410-428.

Kovalenko, V.I., Kozlovsky, A.M., Yarmolyuk, V.V., 2010. Comendite-bearing subduction-related volcanic associations in the Khan-Bogd Area, Southern Mongolia: Geochemical Data. Petrology 18, 571-595.

Kramers, J.D., Tolstikhin, I.N., 1997. Two terrestrial lead isotope paradoxes, forward transport modeling, core formation and the history of the continental crust. Chemical Geology 139, 75-110.

Lecca, L., Lonis, R., Luxoro, S., Melis, E., Secchi, F., Brotzu, P., 1997. Oligo-Miocene volcanic sequences and rifting stages in Sardinia: a review. Periodico di Mineralogia 66, 7-61.

Le Maitre, R.W., 2005. Igneous rocks. A classification and glossary of terms. Second Edition. Recommendations of the International Union of Geological Sciences Subcommission on the Systematics of Igneous Rocks. Cambridge University Press, Cambridge, 236 pp.

Liew, T.C., Milisenda, C.C., Hofmann, A.W., 1991. Isotopic contrasts, chronology of elemental transfers and high-grade metamorphism: the Sri Lanka Highland granulites, and the Lewisian (Scotland) and Nuk (SW Greenland) gneisses. Geologische Rundschau 80, 279-288.

Liu, Y., Gao, S., Yuan, H., Zhou, L., Liu, X., Wang, X., Hu, Z., Wang, L., 2004. U-Pb zircon ages and Nd, Sr, and Pb isotopes of lower crustal xenoliths from North China Craton: insights on evolution of lower continental crust. Chemical Geology 211, 87-109.

Lustrino, M., 2005. How the delamination and the detachment of lower continental crust can influence basaltic magmatism. EarthScience Reviews 72, 21-38.

Lustrino, M., 2011. What "anorogenic" igneous rocks can tell us about the chemical composition of the upper mantle: case studies from the circum-Mediterranean area. Geological Magazine, 148, 304-316.

Lustrino, M., Brotzu, P., Lonis, R., Melluso, L., Morra, V., 2004a. European subcontinental manltle as revealed by Neogene volcanic rocks and mantle xenoliths of Sardinia. Field trip guide, IGC Florence 2004.

Lustrino, M., Cucciniello, C., Melluso, L., Tassinari, C.C.G., de Gennaro, R., Serracino, M., 2012. Petrogenesis of Cenozoic volcanic rocks in the NW sector of the Gharyan volcanic field, Libya. Lithos, 155, 218-235.

Lustrino, M., Dallai, L., 2003. On the origin of EM-I end-member. Neues Jahrbuch für Mineralogie Abhandlungen 179, 85-100.

Lustrino, M., Duggen, S., Rosenberg, C.L., 2011. The Central-Western Mediterranean: Anomalous igneous activity in an anomalous collisional setting. Earth-Science Reviews 104, 1-40.

Lustrino, M., Melluso, L., Morra, V., 1999. Origin of glass and its relationships with phlogopite in mantle xenoliths from central Sardinia (Italy). Periodico di Mineralogia 68, 13-42.

Lustrino, M., Melluso, L., Morra, V., 2000. The role of lower continental crust and lithospheric mantle in the genesis of Plio-Pleistocene volcanic rocks from Sardinia (Italy). Earth and Planetary Science Letters 180, 259-270.

Lustrino, M., Melluso, L., Morra, V., 2002. The transition from alkaline to tholeiitic magmas: a case study from the Orosei-Dorgali Pliocene volcanic district (NE Sardinia, Italy). Lithos 63, 83-113.

Lustrino, M., Melluso, L., Morra, V., 2007a. The geochemical peculiarity of "Plio-Quaternary" volcanic rocks of Sardinia in the circum-Mediterranean area, in: Beccaluva, L., Bianchini, G., Wilson, M. (Eds.), Cenozoic Volcanism in the Mediterranean Area. Geological Society of America Special Paper 418, 277-301.

Lustrino, M., Melluso, L., Morra, V., Secchi, F., 1996. Petrology of Plio-Quaternary volcanic rocks from central Sardinia. Periodico di Mineralogia 65, 275-287.

Lustrino, M., Morra, V., Fedele, L., Franciosi, L., 2009. Beginning of the Apennine subduction system in central western Mediterranean: Constraints from Cenozoic "orogenic" magmatic activity of Sardinia, Italy. Tectonics 28, TC5016, doi:10.1029/2008TC002419.

Lustrino, M., Morra, V., Fedele, L., Serracino, M., 2007b. The transition between "orogenic" and "anorogenic" magmatism in the western Mediterranean area: the Middle Miocene volcanic rocks of Isola del Toro (SW Sardinia, Italy). Terra Nova 19, 148-159.

Lustrino, M., Morra, V., Melluso, L., Brotzu, P., d'Amelio, F., Fedele, L., Franciosi, L., Lonis, R., Petteruti Liebercknecht, A.M., 2004b. The Cenozoic igneous activity of Sardinia. Periodico di Mineralogia 73, 105-134.

Lustrino, M., Wilson, M., 2007. The circum-Mediterranean anorogenic Cenozoic igneous province. Earth-Science Reviews 81, 1-65.

Lyubetskaya, T., Korenaga, J., 2007. Chemical composition of Earth's primitive mantle and its variance: 1. Methods and results. Journal of Geophysical Research 112, B03211. doi:10.1029/2005JB004223.

Mattey, D., Lowry, D., MacPherson, C., 1994. Oxygen isotope composition of mantle peridotite. Earth and Planetary Science Letters 128, 231-241.

Mattioli, M., Guerrera, F., Tramontana, M., Raffaelli, G., D'Atri, M., 2000. High-Mg tertiary basalts in southern Sardinia (Italy). Earth and Planetary Science Letters 179, 1-7.

Médard, E., Schmidt, M.W., Schiano, P., 2004. Liquidus surfaces of ultracalcic primitive melts: formation conditions and sources. Contributions to Mineralogy and Petrology 148, 201-215.

Meisel, T., Moser, J., Fellner, N., Wegscheider, W., Schoenberg, R., 2001. Simplified method for the determination of Ru, Pd, Re, Os, Ir and Pt in chromitites and other geological materials by isotope dilution ICP-MS and acid digestion. Analyst 126, 322-328.

Melluso, L, Morra, V, Brotzu, P, Tommasini, S, Renna, M.R., Duncan, R.A., Franciosi, L, d'Amelio, F., 2005. Geochronology and petrogenesis of the Cretaceous Antampombato-Ambatovy complex and associated dyke swarm, Madagascar. Journal of Petrology 46, 1963-1996

Miyashiro, A., 1974. Volcanic rock series in island arcs and active continental margins. American Journal of Science 274, 321-355.

Molli, G., Malavieille, J., 2011. Orogenic processes and the Corsica/Apennines geodynamic evolution: insights from Taiwan. International Journal of Earth Sciences 5, 1207-1224.

Montanini, A., Barbieri, M., Castorina, F., 1994. The role of fractional crystallization, crustal melting and magma mixing in the petrogenesis of rhyolites and mafic inclusion-bearing dacites from the Monte Arci volcanic complex (Sardinia, Italy). Journal of Volcanology and Geothermal Research 61, 95-120.

Morra, V., Secchi, F.A., Assorgia, A., 1994. Petrogenetic significance of peralkaline rocks from Cenozoic calcalkaline volcanism from SW Sardinia, Italy. Chemical Geology 118, 109-142.

Morra, V., Secchi, F.A.G., Melluso, L., Franciosi, L., 1997. High-Mg subduction related Tertiary basalts in Sardinia, Italy. Lithos 40, 69-91.

Mungall, J.E., Martin, R.F., 1995. Petrogenesis of basalt-comendite and basalt-pantellerite suites, Terceira, Azores, and some implications for the origin of oceanic rhyolites. Contributions to Mineralogy and Petrology 119, 43-55.

Nier, A.O., 1937. The isotopic constitution of osmium. Physical Review, 52, 885.

Niida, K., Green, D.H., 1999. Stability and chemical composition of pargasitic amphibole in MORB pyrolite under upper mantle conditions. Contributions to Mineralogy and Petrology 135, 18-40.

Nowell, G.M., Kempton, P.D., Noble, S.R., Fitton, J.G., Saunders, A.D., Mahoney, J.J., Taylor, R.N., 1998. High precision Hf isotope measurements of MORB and OIB by thermal ionisation mass spectrometry: Insights into the depleted mantle. Chemical Geology 149, 211-233.

Peccerillo, A., Lustrino, M., 2005. Compositional variations of the Plio-Quaternary magmatism in the circum-Tyrrhenian area: deep- versus shallow-mantle processes, in: Foulger, G.R., Natland, J.H., Presnall, D.C., Anderson, D.L. (Eds.), Plates, Plumes & Paradigms. Geological Society of America Special Papers 388, 421-434.

Peng, Z.X., Mahoney, J.J., 1995. Drillhole lavas from the northwestern Deccan Traps, and the evolution of Réunion hotspot mantle. Earth and Planetary Science Letters 134, 169-185.

Pfander, J.A., Jung, S., Munker, C., Stracke, A., Mezger, K., 2012. A possible high Nb/Ta reservoir in the continental lithospheric mantle and consequences on the global Nb budget – Evidence from continental basalts from Central Germany. Geochimica et Cosmochimica Acta 77, 232-251.

Qian, Q., Hermann, J., 2013. Partial melting of lower crust at 10-15 kbar: constraints on adakite and TTG formation. Contribution to Mineralogy and Petrology 165, 1195-1224.

Rapp, R.P., Watson, E.B., 1995. Dehydration melting of metabasalt at 8-32 kbar: implications for continental growth and crust-mantle recycling. Journal of Petrology 36,891-931.

Réhault, J.-P., Honthaas, C., Guennoc, P., Bellon, H., Ruffet, G., cotton, J., Sosson, M., Maury, R.C., 2012. Offshore Oligo-Miocene volcanic fields within the Corsica-Liguria Basin: magmatic diversity and slab evolution in the western Mediterranean Sea. Journal of Geodynamics 58, 73-95.

Reisberg L., Meisel T., 2002. The Re-Os Isotopic System: A Review of Analytical Techniques. Geostandards Newsletters, 26, 249-267.

Riguzzi, F., Panza, G., Varga, P., Doglioni, C., 2010. Can Earth's rotation and tidal despinning drive plate tectonics? Tectonophysics 484, 60-73.

Rocco, I., Lustrino, M., Morra, V., Melluso, L., 2012. Petrological, geochemical and isotopic characteristics of the lithospheric mantle beneath Sardinia (Italy) as indicated by ultramafic xenoliths enclosed in alkaline lavas. International Journal of Earth Sciences 101, 1111-1125.

Ronga, F., 2011. Petrogenesi delle vulcaniti del Sulcis (Sardegna sud-occidentale). Unpublished PhD thesis, University of Naples Federico II, 168 pp.

Ronga, F., Lustrino, M., Marzoli, A., Melluso, L., 2010. Petrogenesis of a basalt-comendite-pantellerite rock suite: the Boseti volcanic complex (Main Ethiopian Rift). Mineralogy and Petrology 98, 227-243.

Rosenbaum, G., Lister, G.S., Duboz, C., 2002. Reconsstruction of the tectonic evolution of the Western Mediterranean since the Oligocene. Journal of the Virtual Explorer 8, 107-130.

Rudnick, R.L., Goldstein, S.L., 1990. The Pb isotopic composition of lower crustal xenoliths and the evolution of lower crustal Pb. Earth and Planetary Science Letters 98, 192-207.

Schiano, P., Eiler, J.M., Hutcheon, I.D., Stolper, E.M., 2000. Primitive CaO-rich, silica-undersaturated melts in island arcs: evidence for the involvement of clinopyroxene-rich lithologies in the petrogenesis of arc magmas. Geochemistry Geophysics Geosystems 1:1999GC000032.

Schmidt, M.W., Poli, S., 1998. Experimentally based water budgets for dehydrating slabs and consequences for arc magma generation. Earth and Planetary Science Letters 163, 361-379.

Schwab, B.E., Johnston, A.D., 2001. Melting systematics of modally variable, compositionally intermediate peridotites and the effects of mineral fertility. Journal of Petrology 42, 1789-1811.

Sharp, Z.D., 1995. Oxygen isotope geochemistry of the Al_2SiO_5 polymorphs. American Journal of Science 295, 1058-1076.

Shimabukuro, D.H., Wakabayashi, J., Alvarez, W., Chang, S., 2012. Cold and old: the rock record of subduction initiation beneath a continental margin, Calabria, southern Italy. Lithosphere doi:10.1130/L222.1.

Shirey, S.B., Walker, R.J., 1998. The Re-Os isotope system in cosmochemistry and high-temperature geochemistry. Annual Reviews of Earth and Planetary Sciences 26, 423-500.

Smith, I.E.M., Chappel, B.W., Ward, G.K., Freeman, R.S., 1977. Peralkaline rhyolites associated with andesitic arcs of the southwest pacific. Earth and Planetary Science Letters 37, 230-236.

Speranza, F., Villa, I.M., Sagnotti, L., Florindo, F., Cosentino, D., Cipollari, P., Mattei, M., 2002. Age of the Corsica-Sardinia rotation and Liguro-Provençal Basin spreading: new paleomagnetic and Ar/Ar evidence. Tectonophysics 347, 231-251.

Stracke, A., Hofmann, A.W., Hart, S.R., 2005. FOZO, HIMU, and the rest of the mantle zoo. Geochemistry Geophysics Geosystems 6, doi:10.1029/2004GC000824.

Stracke, A., 2012. Earth's heterogeneous mantle: a product of convection-driven interaction between crust and mantle. Chemical Geology 330-331, 274-299.

Syracuse, E.M., Abers, G.A., 2006. Global compilation of variations in slab depth beneath arc volcanoes and implications. Geochemistry Geophysics Geosystems 7, doi: 10.1029/2005GC001045.

Todt, W., Cliff, R.A., Hanser, A., Hoffmann, A.W., 1996. Evaluation of a ^{202}Pb-^{205}Pb double spike for high precision lead isotopic analysis, In Basu, A.R., Hart, S.R. (Eds.), Earth Processes: Reading the Isotopic Code. Geophysical Monograph Series American Geophysical Union 95, 429-437.

Tommasini S., Poli G., Halliday A.N., 1995. The role of sediment subduction and crustal growth in Hercynian plutonism: isotopic and trace element evidence from the Sardinia-Corsica batholith. Journal of Petrology, 36, 1305-1332.

Turpin L., Velde D., Pinte G., 1988. Geochemical comparison between minettes and kersantites from the Western European Hercynian orogen: trace element and Pb-Sr-Nd isotope constraints on their origin. Earth and Planetary Science Letters, 87, 73-86.

Trua, T., Serri, G., Marani, M., 2007. Geochemical features and geodynamic significance of the southern Tyrrhenian backarc basin. Geological Society of America Special Paper 418, 221-233.

Ulfbeck, D., Baker, J., Waight, T., Krogstad, E., 2003. Rapid sample digestion by fusion and chemical separation of Hf for isotopic analysis by MC-ICPMS. Talanta 59, 365-373.

van Acken, D., Becker, H., Walker, R.J., McDonough, W.F., Wombacher, F., Ash, R.D., Piccoli, P.M., 2010. Formation of pyroxenite layers in the Totalp ultramafic massif (Swiss Alps) – Insights from highly siderophile elements and Os isotopes Geochimica et Cosmochimica Acta 74, 661-683.

Vigliotti, L., Langenheim, V.E., 1995. When did Sardinia stop rotating? New paleomagnetic results. Terra Nova 7, 424-435.

Walkzyk, T., Hebeda, E.H., Heumann, K.G., 1991. Osmium isotope ratio measurements by negative thermal ionization mass spectrometry (NTI-MS). Fresnius Journal of Analytical chemistry, 341, 537-541.

Walker, R.J., 1988. Low-blank chemical separation of Rhenium and Osmium from gram quantities of silicate rock for measurement by resonance ionization mass spectrometry. Analytical Chemistry 60, 1231-1234.

White, W.M., 2010. Oceanic island basalts and mantle plumes: the geochemical perspective. Annual Reviews of Earth and Planetary Sciences 38, 133-160.

White, J.C., Espejel-Garcia, V.V., Anthony, E.Y., Omenda, P.A., 2012. Open system evolution of peralkaline trachyte and phonolite from the Suswa volcano, Kenya rift. Lithos 152, 84-104.

Willbold, A., Stracke, A., 2006. Trace element composition of mantle end-members: Implication for recacyling of oceanic and upper and lower continental crust. Geochemistry Geophysics Geosystems 7, doi:10.1029/2005GC001005.

Zartman, R.E., Haines, S.M., 1988. The plumbotectonic model for Pb isotopic systematics among major terrestrial reservoirs – a case for bi-directional transport. Geochimica et Cosmochimica Acta 52, 1327-1339.

Zeng, G., Chen, L.-H., Hu, S.-L., Xu, X.-S., 2013. Genesis of Cenozoic low-Ca alkaline basalts in the Nanjing basaltic field, eastern China: The case for mantle xenolith-magma interaction. Geochemistry, Geophysics, Geosystems 14, doi:10.1002/ggge.20127.

Zheng, Y., 1993. Calculation of oxygen fractionation in anhydrous silicate minerals. Geochimica et Cosmochimica Acta 57, 1079-1091.

Zindler, A., Hart, S. 1986. Chemical geodynamics. Annual Reviews of Earth and Planetary Sciences 14, 493-571.

Figure captions

Fig. 1 = Simplified geological map of Sardinia, showing the main Cenozoic igneous outcrops (modified from Lustrino et al., 2009).

Fig. 2 = General view and cross sections of the western Mediterranean area (modified from Carminati et al., 2010, 2012) at 40 Ma and another at 15 Ma. Sardinia is highlighted in orange. Readers are referred to the web version of the figure.

Fig. 3 = Chronostratigraphy of the main igneous episodes and the most important Cenozoic geodynamic events of the western Mediterranean Sea, with special emphasis on Sardinia (modified from Lustrino et al., 2007b, 2009; Carminati et al. 2012). SR = "Subduction-related" Late Eocene- Middle Miocene igneous rocks; RPV = Radiogenic Pb Volcanics (Lustrino et al., 2000); UPV = Unradiogenic Pb Volcanics (Lustrino et al., 2000).

Fig. 4 = Total Alkali vs. silica diagram (Le Maitre et al., 2005). Triangles: SR volcanic rocks; Squares = RPV rocks; Circles = UPV rocks.

Fig. 5 = FeO*/MgO vs. SiO_2 diagram for SR volcanic rocks of Sardinia. Symbols as in Fig. 4. The two thick lines define three fields (High-Fe, Medium-Fe and Low-Fe) according to Arculus (2003). The red dashed line separates the tholeiitic from the calcalkaline fields (Miyashiro, 1974).

Fig. 6 = (a) $^{143}Nd/^{144}Nd$ vs. $^{87}Sr/^{86}Sr$; (b) $^{207}Pb/^{204}Pb$ vs. $^{206}Pb/^{204}Pb$; (c) $^{208}Pb/^{204}Pb$ vs. $^{206}Pb/^{204}Pb$; (d) $^{87}Sr/^{86}Sr$ vs. $^{206}Pb/^{204}Pb$; (e) $^{143}Nd/^{144}Nd$ vs. $^{206}Pb/^{204}Pb$; (f) $^{176}Hf/^{177}Hf$ vs. $^{143}Nd/^{144}Nd$; (g) $^{176}Hf/^{177}Hf$ vs. $^{87}Sr/^{86}Sr$; (h) $^{176}Hf/^{177}Hf$ vs. $^{206}Pb/^{204}Pb$ diagrams for Cenozoic igneous rocks of Sardinia. The field of the St. Helena basalts (http://georoc.mpch-mainz.gwdg.de/georoc/), considered the classical HIMU-OIB locality, is plotted for comparison. Various estimates of the FOZO mantle end-member are from Stracke et al. (2005).

Fig. 7 = (a) $^{87}Sr/^{86}Sr$ vs. MgO; (b) $^{87}Sr/^{86}Sr$ vs. SiO_2; (c) $^{143}Nd/^{144}Nd$ vs. MgO; (d) $^{143}Nd/^{144}Nd$ vs. SiO_2 diagrams for the Cenozoic igneous rocks of Sardinia. Arrow 1 indicates the increasing effects of interaction of mantle melts with crustal material. Arrow 2 indicates the effects of partial melting of a underplated mafic SR rocks, producing silica-rich melts with unvaried Nd isotopic ratios. Arrow 3 indicates the mixing between crustally contaminated melts (SiO_2 ~60 wt%; $^{143}Nd/^{144}Nd$ ~0.5122) with acid melts produced after partial melting of a basaltic source (SiO_2 ~75 wt%; $^{143}Nd/^{144}Nd$ ~0.5128).

Fig. 8 = (a) $^{187}Os/^{188}Os$ vs. $^{87}Sr/^{86}Sr$; (b) $^{187}Os/^{188}Os$ vs. $^{143}Nd/^{144}Nd$; (c) $^{187}Os/^{188}Os$ vs. $^{206}Pb/^{204}Pb$; (d) $^{187}Os/^{188}Os$ vs. $^{176}Hf/^{177}Hf$ diagrams for the Cenozoic igneous rocks of Sardinia. Samples of other Cenozoic volcanic rocks from Germany (Rhon, Vogelsberg, Urach and Bad Egau; Blusztajn and Hegner, 2002; Jung et al., 2005; 2011; Pfander et al., 2012) and Italy (Roman and Tuscan Provinces; Gasperini et al., 2002; Conticelli et al., 2007) are reported for comparison. The Italian subduction-related rocks plot towards very radiogenic Sr and unradiogenic Nd isotopic compositions, indicated by the arrow in Fig. 8a and a square bracket in Fig. 8b.

Fig. 9 = $^{143}Nd/^{144}Nd$ vs. $^{87}Sr/^{86}Sr$ diagram for the SR rocks of Sardinia. Three mixing lines are drawn, with numbers in italics indicating the degrees of interaction between the two end-members. Thick line: mixing line between a DMM-like source ($^{87}Sr/^{86}Sr$ = 0.70265 and Sr = 12 ppm; $^{143}Nd/^{144}Nd$ = 0.51320 and Nd = 1 ppm) and Atlantic-type sediment ($^{87}Sr/^{86}Sr$ = 0.7200 and Sr = 80 ppm; $^{143}Nd/^{144}Nd$ = 0.51202 and Nd = 40 ppm; Downes et al., 2001). The yellow star indicates the isotopic composition of the EM-II end-member (Zindler and Hart, 1986).

Dotted line: mixing line between a primitive basaltic melt (sample KB23 from Montresta district, Morra et al., 1997; $^{87}Sr/^{86}Sr$ = 0.70398 and Sr = 450 ppm; $^{143}Nd/^{144}Nd$ = 0.51271 and Nd = 9.2 ppm) and a mafic Hercynian lamprophyre (sample W9A1m, Turpin et al., 1988; $^{87}Sr/^{86}Sr$ = 0.70795 and Sr = 223 ppm; $^{143}Nd/^{144}Nd$ = 0.51265 and Nd = 16.6 ppm). Dashed line: mixing line between a primitive basaltic melt (sample KB23) and an acid Hercynian granitoid (sample SP241, Tommasini et al., 1995; $^{87}Sr/^{86}Sr$ = 0.71661 and Sr = 185 ppm; $^{143}Nd/^{144}Nd$ = 0.51215 and Nd = 30 ppm). The Sr-Nd isotopic composition of the potential Hercynian contaminant has been recalculated at 20 Ma.

Fig. 10 = Primitive Mantle-normalized (Lyubetskaya and Korenaga 2007) multielemental diagram for SR (a), RPV (b) and UPV (c) rocks. The field of the St. Helena basalts (http://georoc.mpch-mainz.gwdg.de/georoc/), considered the classical HIMU-OIB locality, is plotted for comparison.

Fig. 11 = $^{207}Pb/^{206}Pb$ vs. $^{208}Pb/^{206}Pb$ diagram for the Cenozoic igneous rocks of Sardinia. The field of St. Helena basalts (http://georoc.mpch-mainz.gwdg.de/georoc/), considered the HIMU-OIB type locality, and various estimates of the FOZO mantle component (Stracke et al., 2005) are reported for comparison.

Fig. 12 = CaO vs. SiO_2 for the Cenozoic igneous rocks of Sardinia.

Table caption

Table 1 = Major element (wt%), trace element (ppm, except Re and Os, reported in ppb) and Sr-Nd-Pb-Hf-Os-O isotopic ratios of the Cenozoic igneous rocks of Sardinia. New data are reported in bold. SR = Subduction-related (Late Eocene-Middle Miocene); RPV = Radiogenic Pb Volcanic Group (11.8-4.4 Ma); UPV = Unradiogenic Pb Volcanic Group (4.8-0.1 Ma). References: 1 = Morra et al. (1997); 2 = Franciosi et al. (2003), 3 = Brotzu et al. (1997); 4 = Lustrino et al. (2009); 5 = Guarino et al. (2011); 6 = Lustrino et al. (2000); 7 = Lustrino et al. (2007a); 8 = Lustrino et al. (2007b); 9 = Lustrino et al. (2002); 10 = This paper. The full list of Sardinian whole-rock analyses (about 1400 samples) can be requested to the first author.

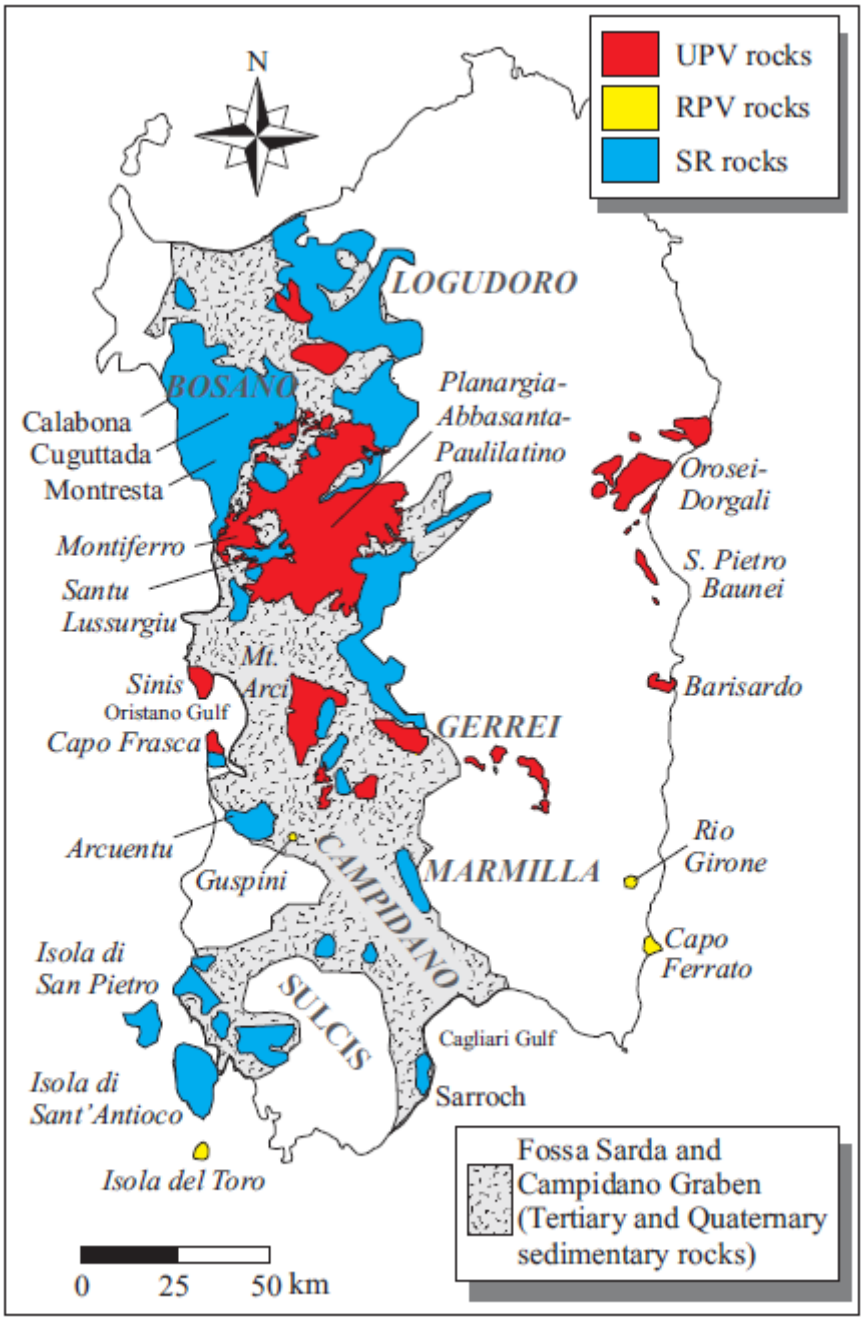

Lustrino et al. (Fig.1)

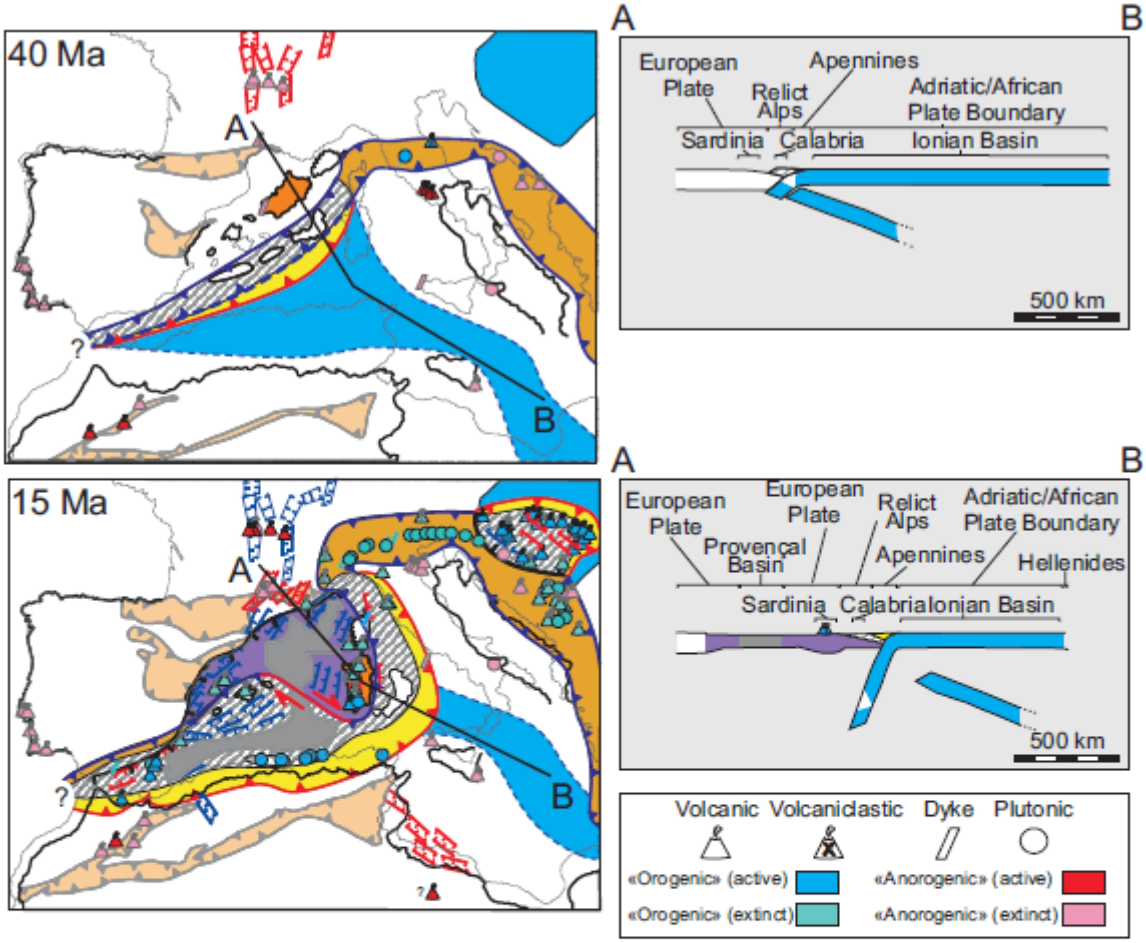

Lustrino et al. (Fig.2)

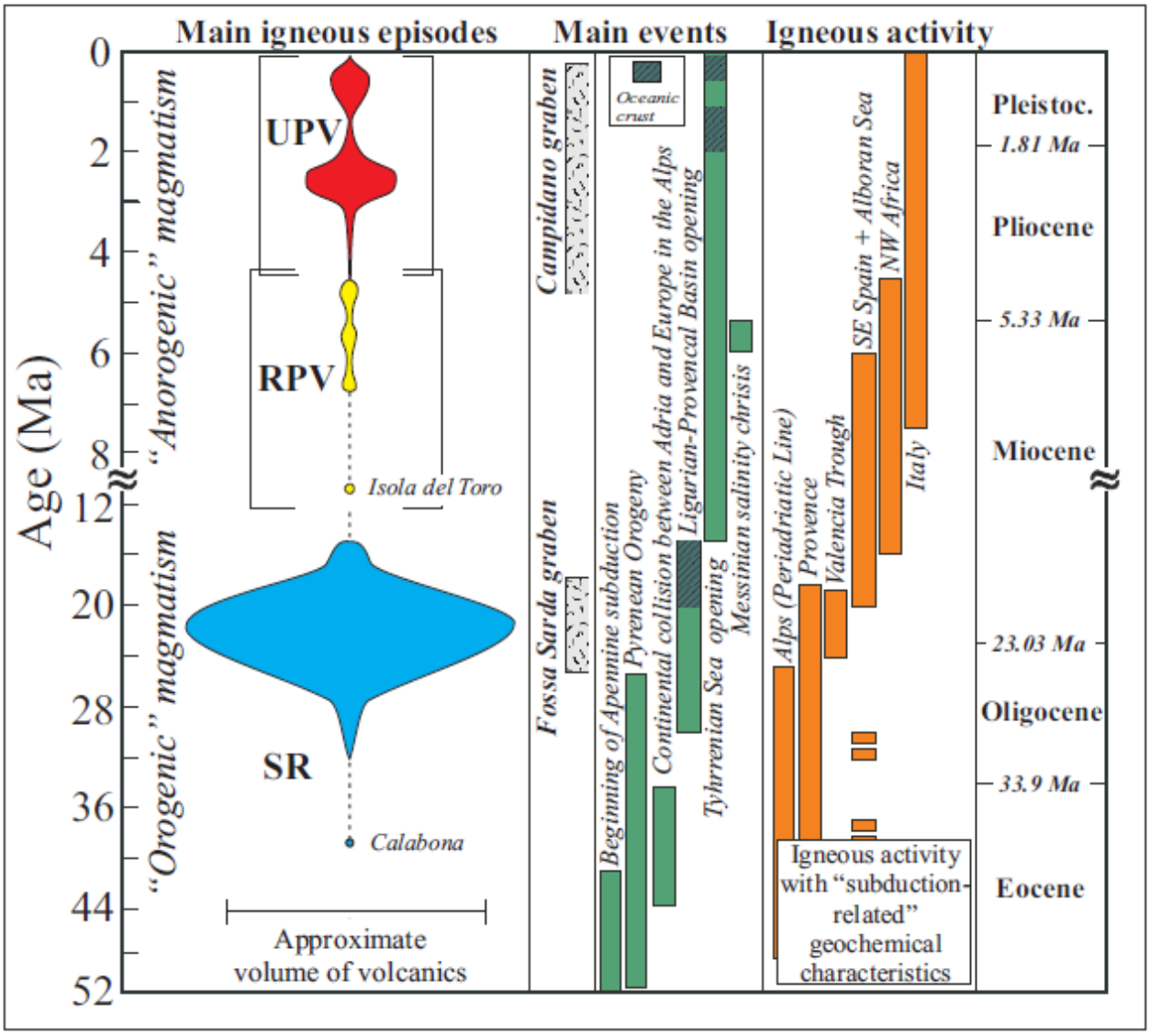

Lustrino et al. (Fig.3)

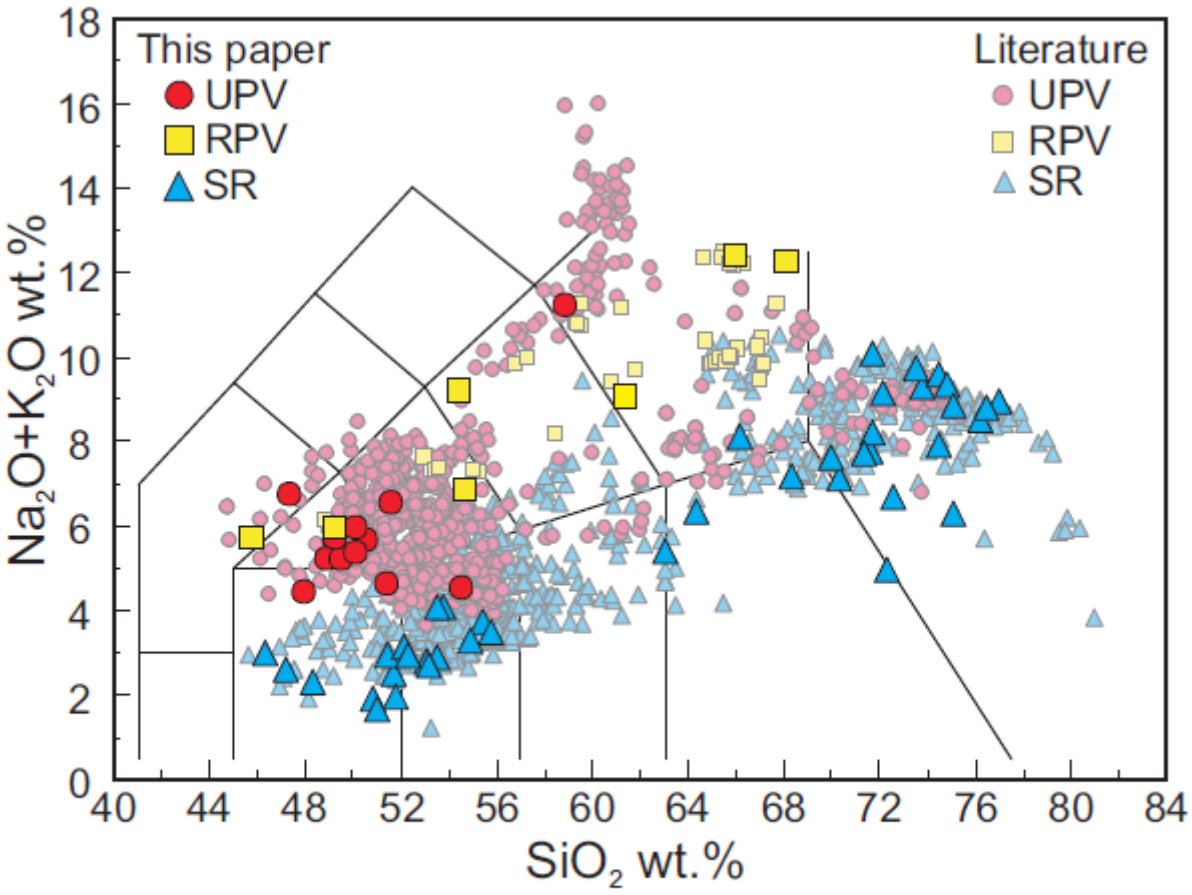

Lustrino et al. (Fig.4)

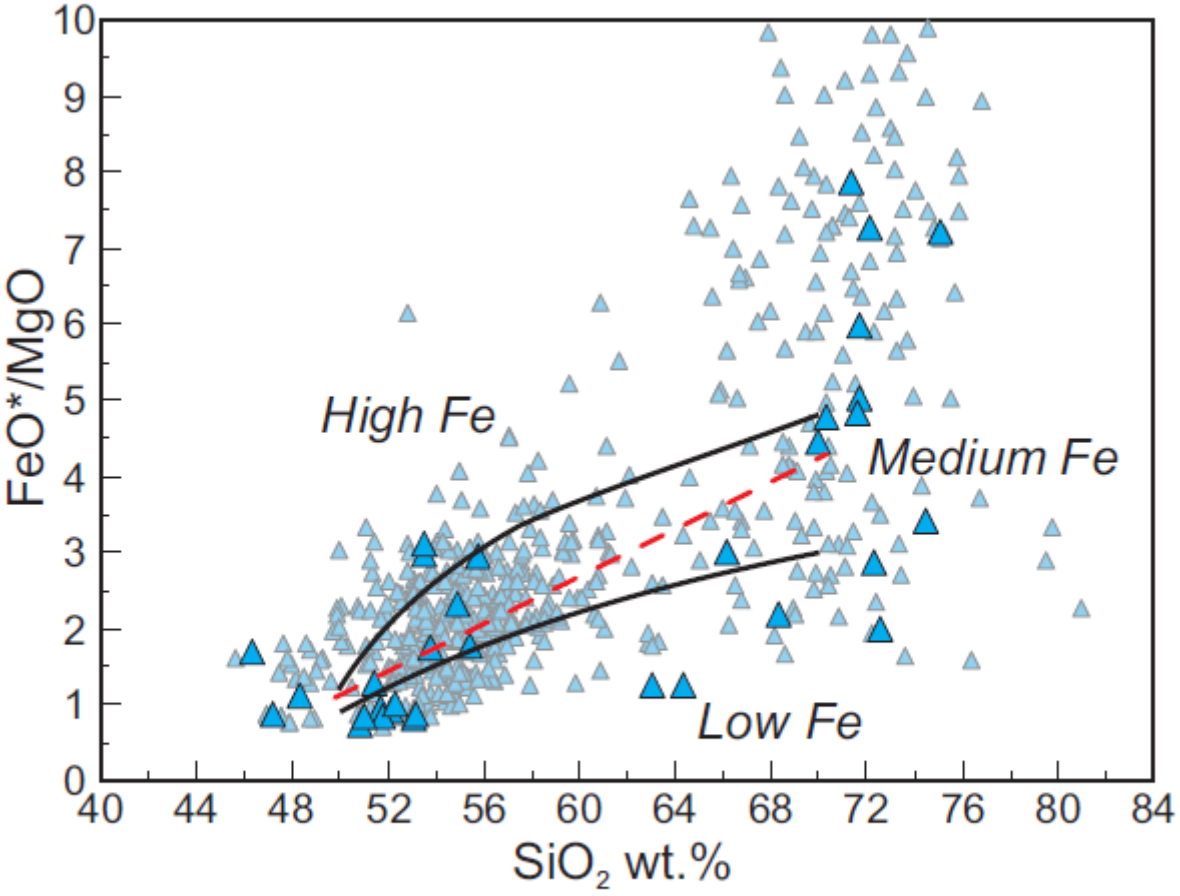

Lustrino et al. (Fig.5)

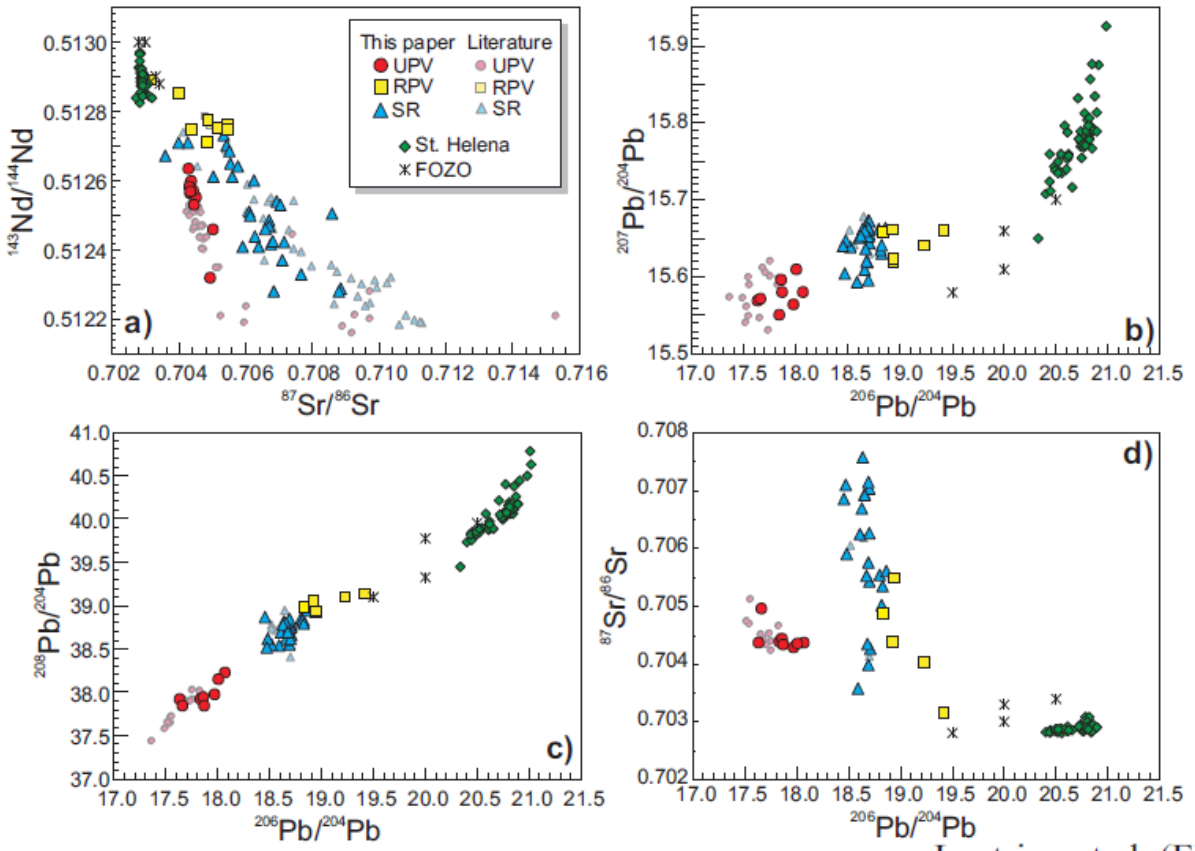

Lustrino et al. (Fig. 6)

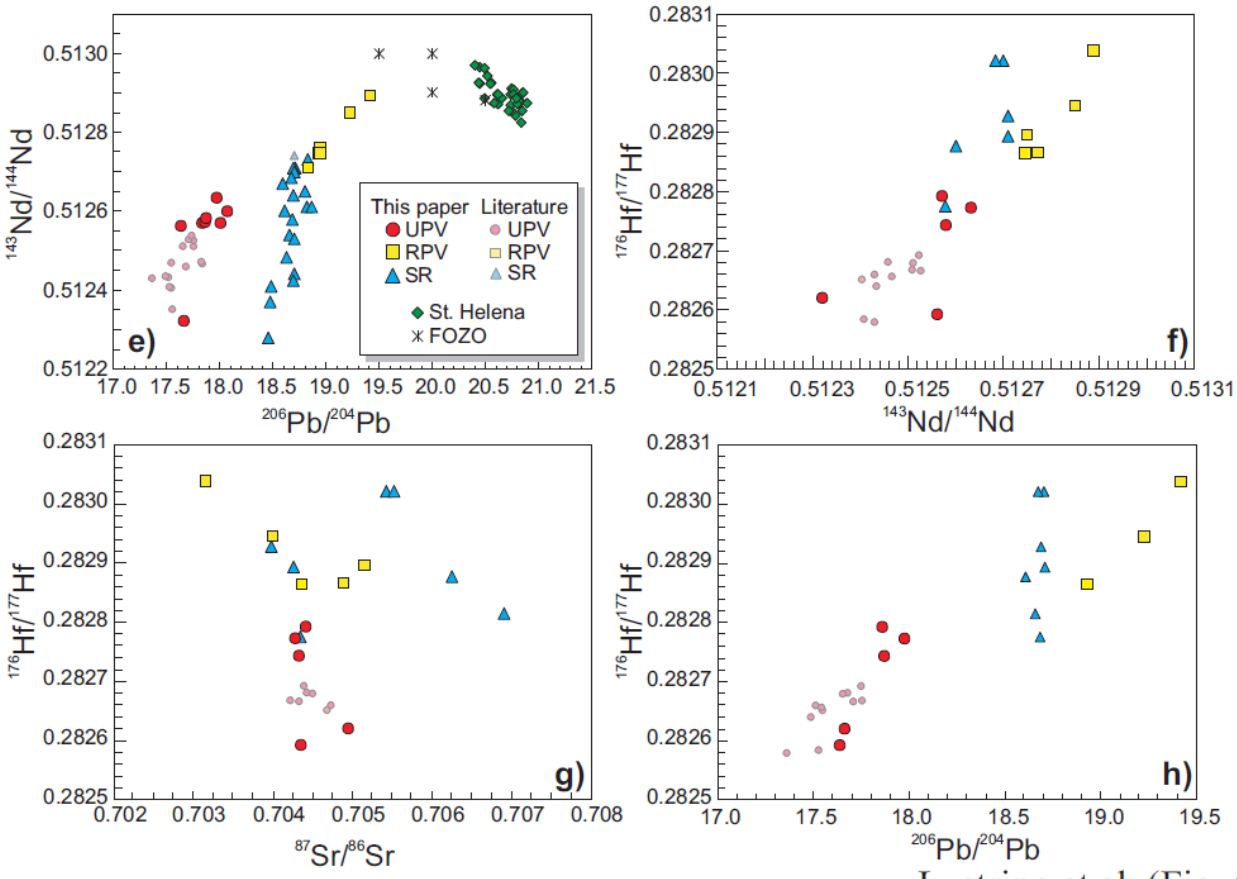

Lustrino et al. (Fig. 6)

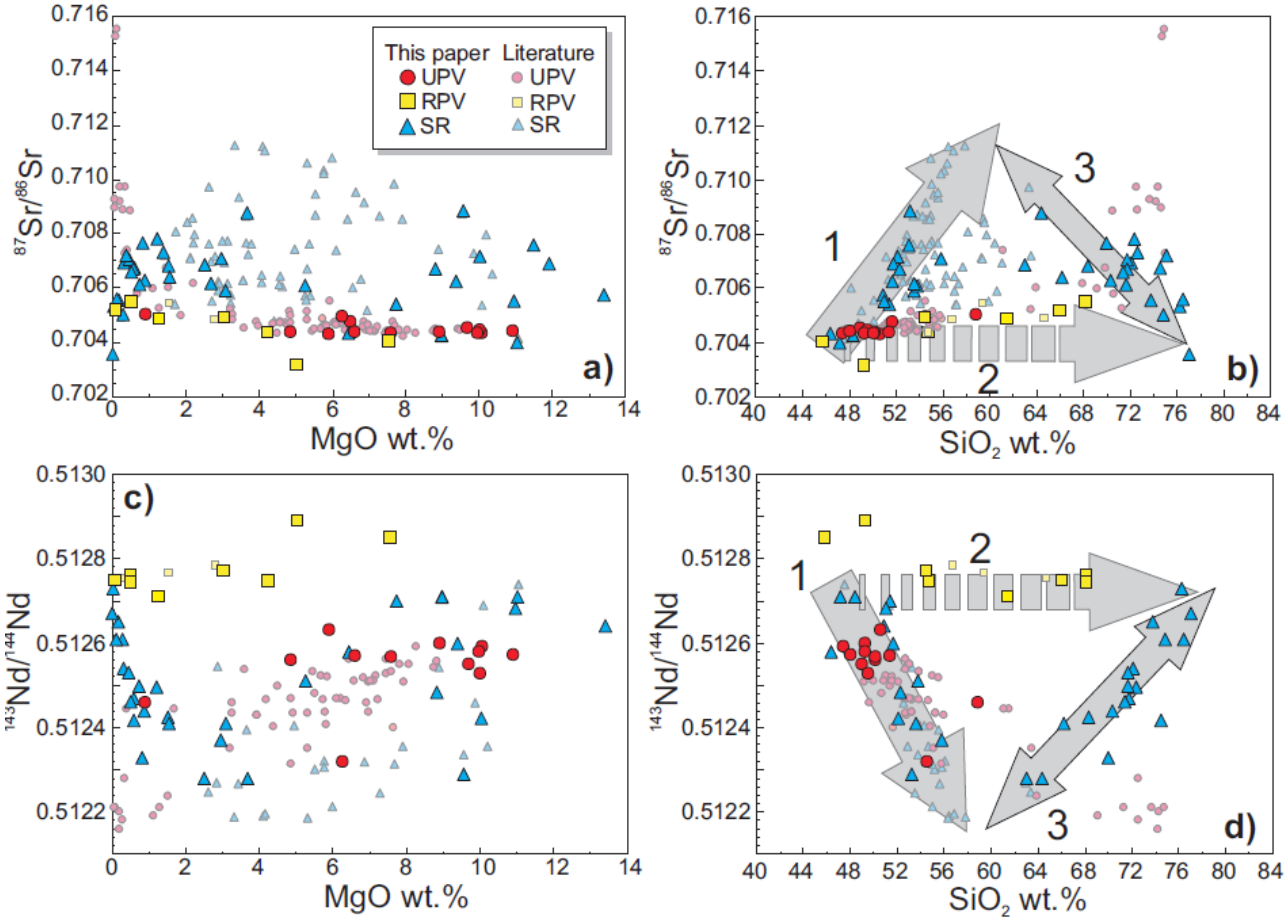

Lustrino et al. (Fig.7)

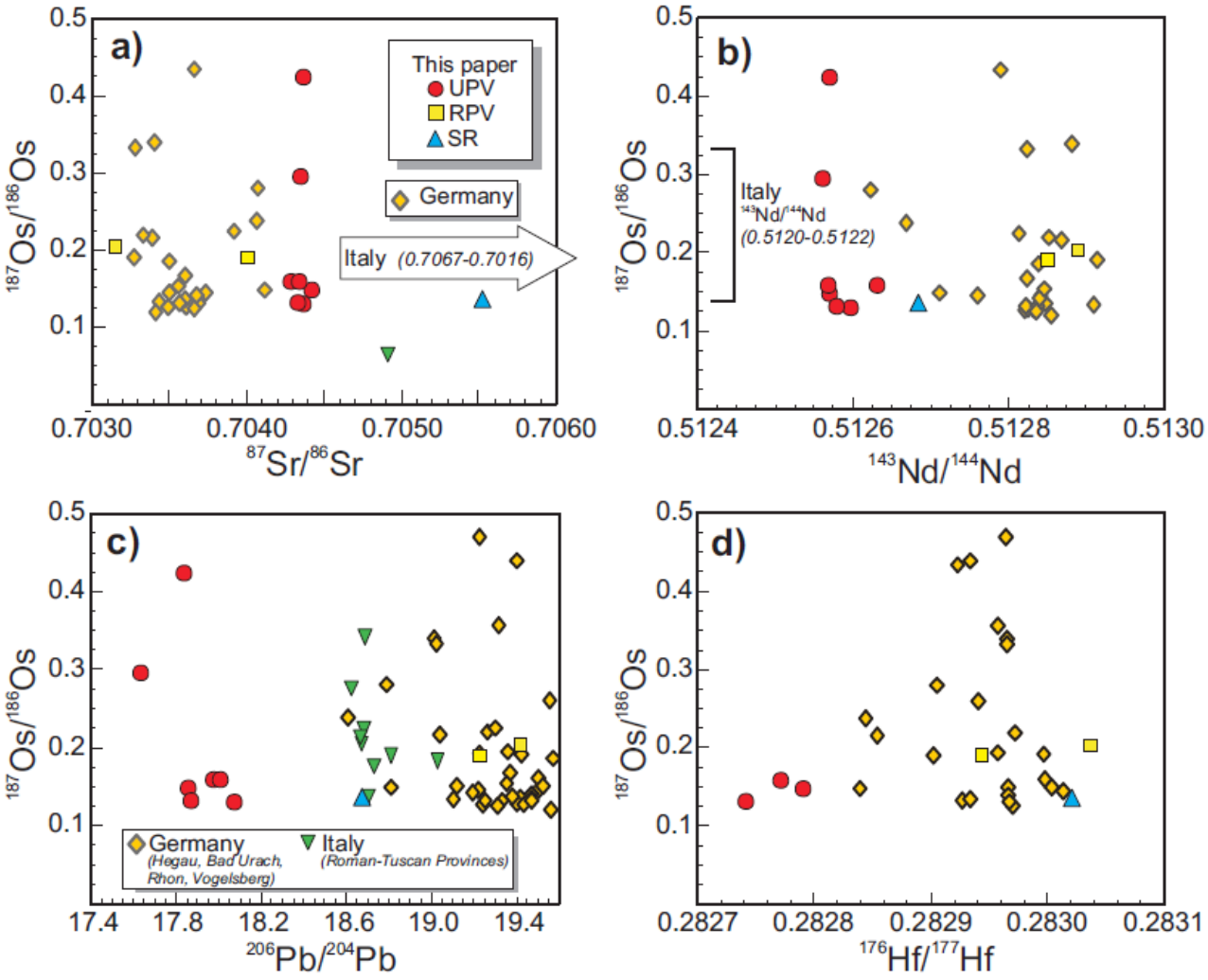

Lustrino et al. (Fig. 8)

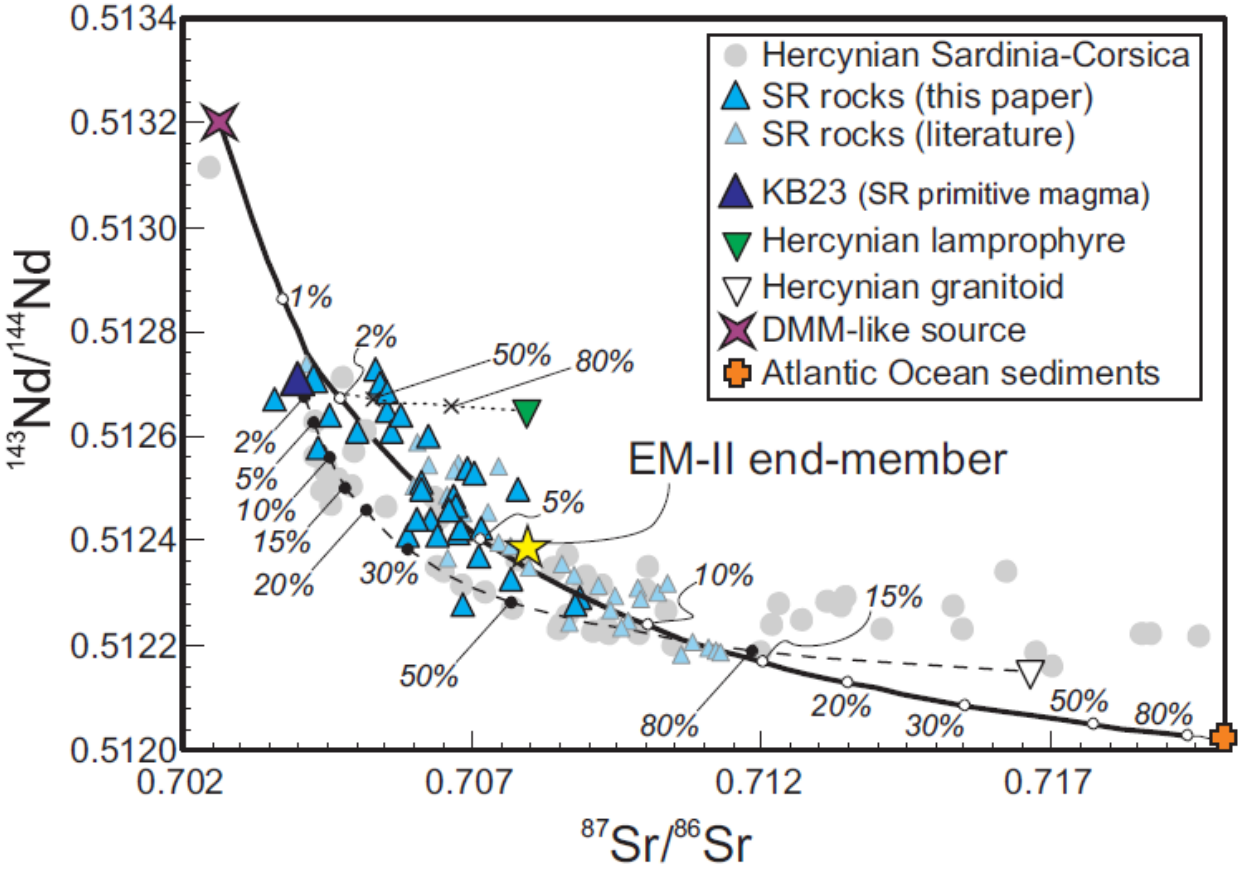

Lustrino et al. (Fig.9)

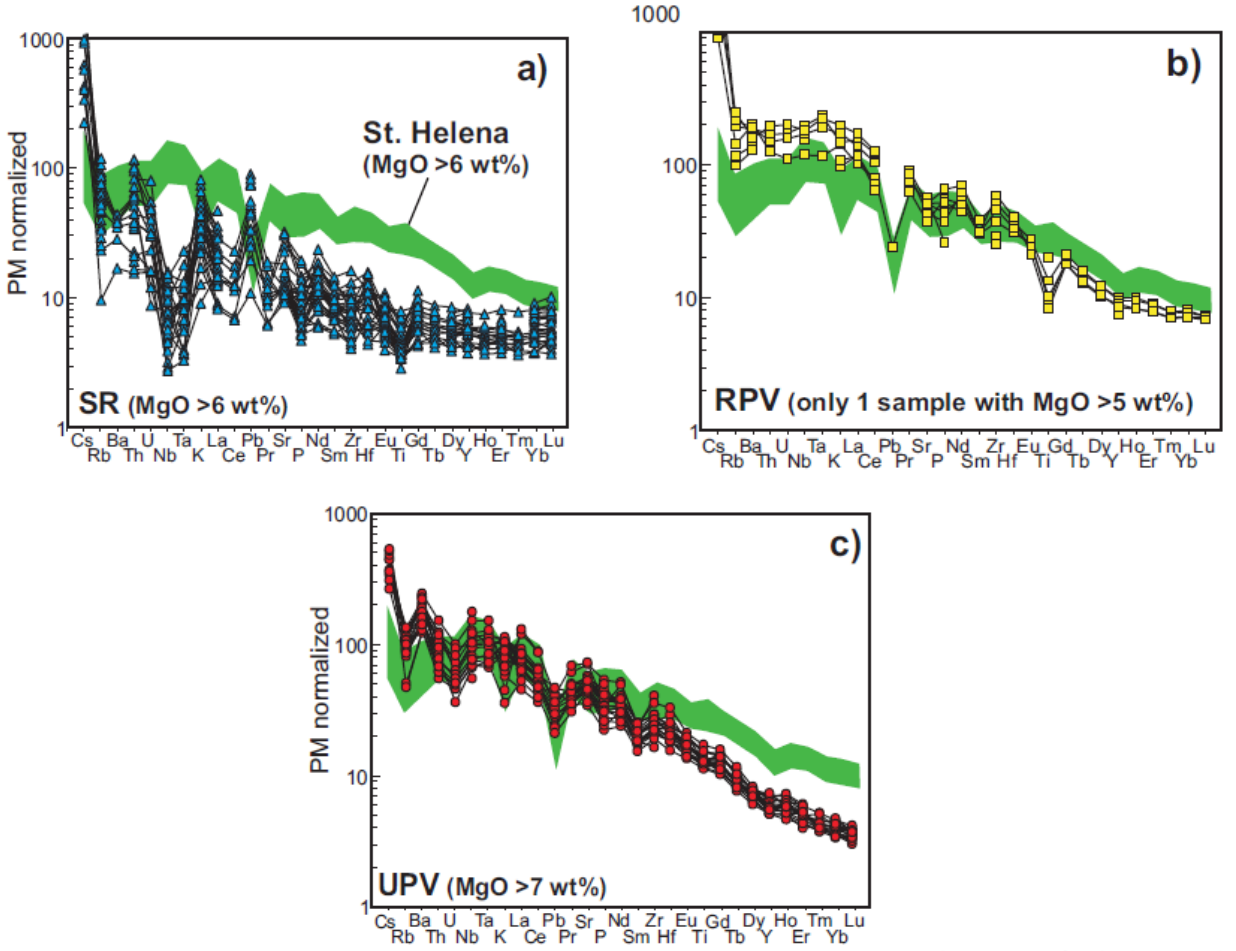

Lustrino et al. (Fig. 10)

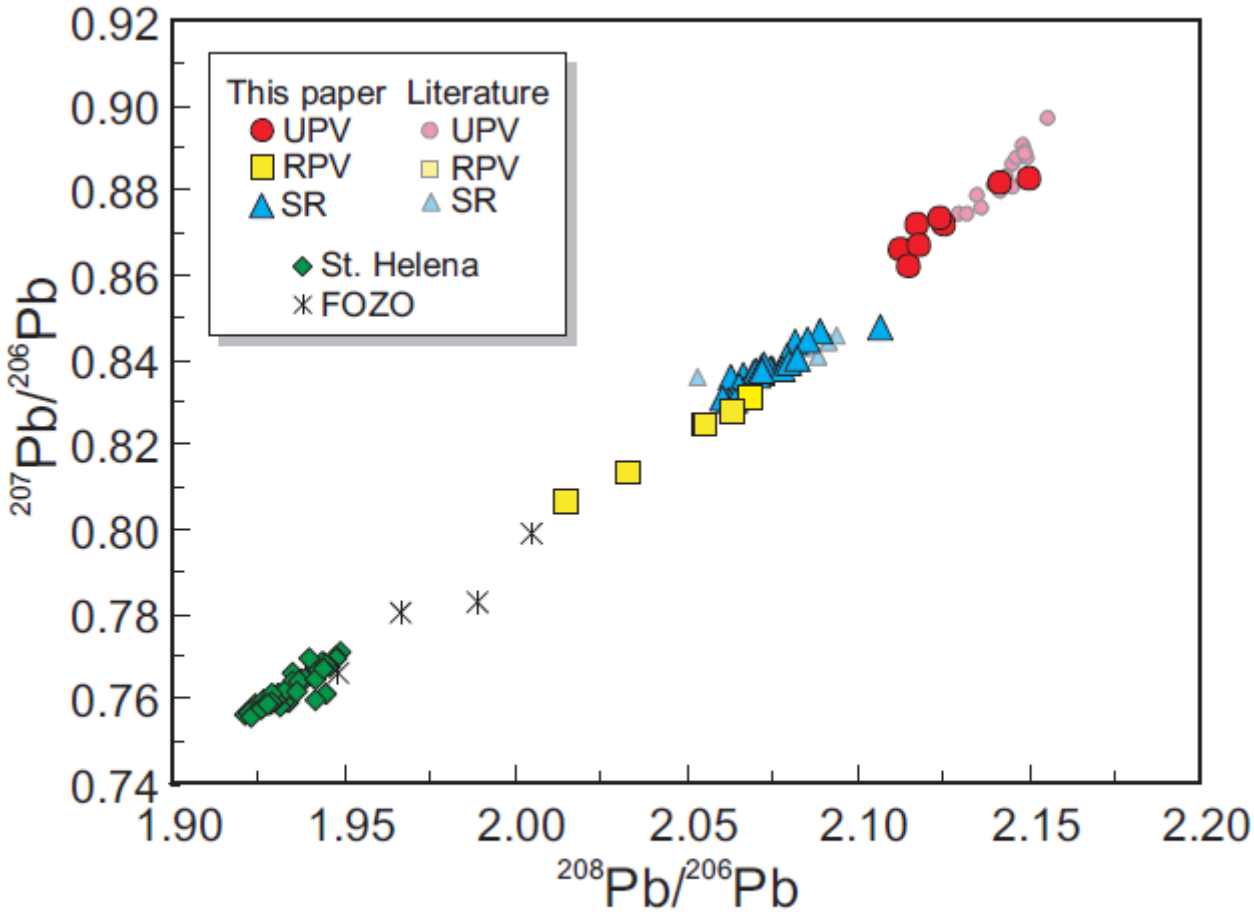

Lustrino et al. (Fig. 11)

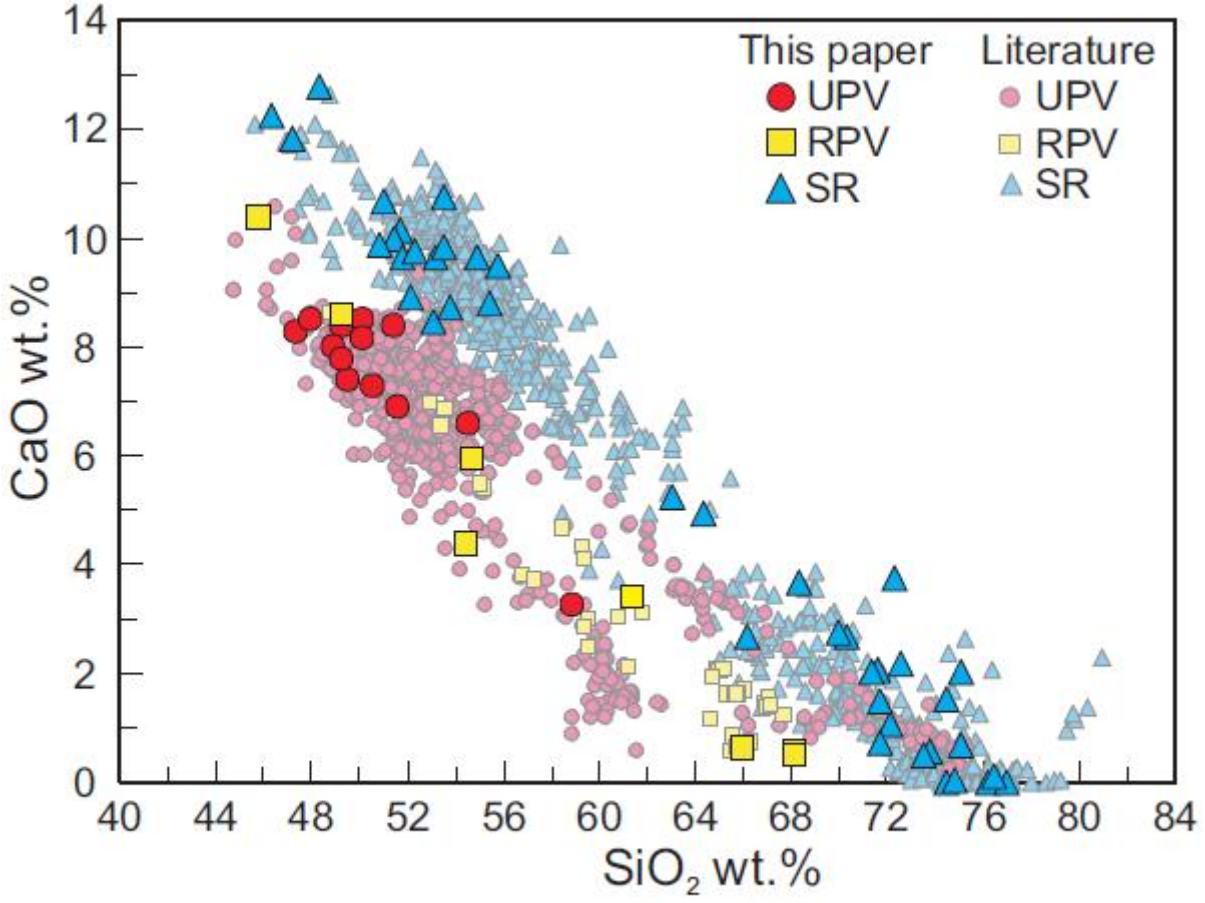

Lustrino et al. (Fig.12)

Table 1

Sheet1

Series	Label	*Ref.*	*Locality*	*Rock Type (TAS)*	Age	SiO_2	TiO_2	Al_2O_3	Fe_2O_3	MnO
SR	KB 13	1-2-10	Montresta	Tholeiitic Basalt	24-16 Ma	48.33	0.74	15.38	11.16	0.12
SR	KB 23	1-2-10	Montresta	Tholeiitic Basalt	24-16 Ma	47.15	0.77	15.36	10.81	0.19
SR	GK 54	10	Sulcis	Basaltic Andesite	21 Ma	**54.56**	**0.80**	**17.99**	**8.23**	**0.14**
SR	GK 55	10	Sulcis	Rhyolite	18 Ma	**68.45**	**0.52**	**13.20**	**4.58**	**0.05**
SR	GK 45	10	Sulcis	Rhyolite	18 Ma	**70.97**	**0.52**	**13.94**	**2.55**	**0.03**
SR	GK 50	10	Sulcis	Rhyolite	15 Ma	**73.00**	**0.35**	**13.17**	**2.41**	**0.03**
SR	GK 51	10	Sulcis	Rhyolite	16 Ma	**73.64**	**0.18**	**12.09**	**3.15**	**0.10**
SR	GK 69	10	Sulcis	Rhyolite	16 Ma	**74.09**	**0.19**	**11.95**	**3.16**	**0.09**
SR	GK 9	10	Sulcis (S. Pietro)	Rhyolite	15 Ma	**72.62**	**0.38**	**13.52**	**2.01**	**0.03**
SR	GK 29	10	Sulcis (S. Pietro)	Rhyolite	16 Ma	**76.13**	**0.25**	**9.59**	**5.27**	**0.10**
SR	GK 109	10	Sulcis (S. Pietro)	Rhyolite	18 Ma	**70.46**	**0.46**	**13.74**	**2.51**	**0.03**
SR	GK 119	10	Sulcis (S. Pietro)	Rhyolite	16 Ma	**75.64**	**0.16**	**10.44**	**3.11**	**0.09**
SR	GK 86	10	Sulcis (S. Antioco)	Rhyolite	15 Ma	**74.27**	**0.24**	**12.41**	**2.27**	**0.06**
SR	GK 84A	10	Sulcis (S. Antioco)	Rhyolite	16 Ma	**75.57**	**0.20**	**10.85**	**3.16**	**0.09**
SR	GK 92	10	Sulcis (S. Antioco)	Basaltic Andesite	21 Ma	**53.27**	**0.92**	**17.20**	**9.23**	**0.14**
SR	V 1	10	Sulcis (Vacca)	Basaltic Andesite	21 Ma	**52.43**	**1.01**	**17.79**	**9.98**	**0.14**
SR	V 5	10	Sulcis (Vacca)	Basaltic Andesite	22 Ma	**54.25**	**1.01**	**16.83**	**9.39**	**0.15**
SR	AR 280	2-3-10	Arcuentu	Tholeiitic Basalt	30-17 Ma	51.67	0.76	15.38	9.87	0.18
SR	RL 116	2-3-10	Arcuentu	Tholeiitic Basalt	30-17 Ma	51.40	0.64	16.02	10.99	0.18
SR	GFC 24	10	Arcuentu	Basaltic Andesite	30-17 Ma	**53.11**	**0.69**	**12.70**	**10.39**	**0.16**
SR	GFC 38b	4-10	Arcuentu	Basaltic Andesite	*17.27 Ma*	**52.10**	**0.66**	**14.34**	**10.47**	**0.18**
SR	GFC 18	4-10	Arcuentu	Tholeiitic Basalt	*20.77 Ma*	**50.86**	**0.53**	**12.31**	**10.79**	**0.19**
SR	MAL 28	10	Marmilla	Basaltic Andesite	20-17 Ma	**53.19**	**0.70**	**14.61**	**9.28**	**0.17**
SR	GFC 33	10	Marmilla	Tholeiitic Basalt	20-17 Ma	**51.79**	**0.66**	**12.60**	**11.12**	**0.18**
SR	GFC 14	4-10	Marmilla	Basaltic Andesite	*19.60 Ma*	**52.27**	**0.61**	**15.38**	**9.87**	**0.16**
SR	MA 37	5-10	Logudoro-Bosano	Rhyolite	16 Ma	74.51	0.18	12.87	2.27	0.08
SR	MARA 7	5-10	Logudoro-Bosano	Dacite	17 Ma	68.28	0.47	14.87	3.70	0.08

SR	FDCB	4-10	Logudoro-Bosano	Dacite	*38.28 Ma*	63.00	0.43	19.54	3.47	0.08
SR	VITROFIR	10	Logudoro-Bosano	Rhyolite	21 Ma	72.31	0.48	13.24	3.83	0.12
SR	MARA 33	5-10	Logudoro-Bosano	Basaltic Andesite	18 Ma	53.72	0.95	16.61	10.21	0.19
SR	MARA 12	5-10	Logudoro-Bosano	Rhyolite	18 Ma	69.95	0.42	14.12	4.02	0.11
SR	MARA 13	10	Logudoro-Bosano	Dacite	18 Ma	64.32	0.47	14.91	5.08	0.07
SR	MA 25C	10	Logudoro-Bosano	Rhyolite	18 Ma	71.57	0.44	13.29	3.90	0.12
SR	MA 35	5-10	Logudoro-Bosano	Rhyolite	21 Ma	72.59	0.31	13.63	3.09	0.05
SR	MARA 34	5-10	Logudoro-Bosano	Basaltic Andesite	18 Ma	53.49	0.91	19.21	9.34	0.18
SR	MARA 38	5-10	Logudoro-Bosano	Rhyolite	18 Ma	75.05	0.29	12.97	2.85	0.03
SR	GFC 103	4-10	Cuguttada	Tholeiitic Basalt		**46.36**	**1.12**	**18.31**	**12.06**	**0.18**
SR	MA 3	10	Anglona	Trachyte	21 Ma	66.13	0.61	15.48	5.18	0.09
SR	MA 62A	5-10	Mulargia-Macomer	Rhyolite	21 Ma	71.69	0.39	13.62	3.84	0.06
SR	MA 67	5-10	Ottana Graben	Rhyolite	21 Ma	71.30	0.47	13.42	4.34	0.03
SR	MAL 35	10	Oristano Gulf (Capo Frasca)	Tholeiitic Basalt		**50.99**	**0.54**	**14.73**	**10.18**	**0.18**
RPV	CF	6-10	Capo Ferrato	Trachyte	*6.6 Ma*	61.43	0.89	16.81	6.68	0.12
RPV	MAL 3	7-10	Capo Ferrato	Mugearite	6.6-5.0 Ma	54.75	1.46	16.83	8.95	0.18
RPV	ALP 6	6-10	Rio Girone	Basanite	*6.4 Ma*	45.78	3.13	15.21	11.69	0.16
RPV	MGV 249	6-10	Guspini	Hawaiite	*4.4 Ma*	49.26	3.12	15.80	11.35	0.15
RPV	T 1	10	Isola del Toro	Trachyte	11.8 Ma	**67.33**	**0.33**	**15.13**	**2.62**	**0.09**
RPV	T 2	10	Isola del Toro	Trachyte	11.8 Ma	**66.94**	**0.35**	**15.06**	**2.67**	**0.07**
RPV	TRL	8-10	Isola del Toro	Benmoreite	*11.8 Ma*	53.86	2.11	16.98	8.32	0.16
RPV	TR 1	8-10	Isola del Toro	Trachyte	11.8 Ma	65.81	0.43	16.86	3.33	0.14
UPV	MAL 10	7-10	Monte Arci	Hawaiite	3.8-2.6 Ma	50.59	2.38	16.34	11.15	0.14
UPV	GFP92	7-10	Montiferro	Mugearite	3.9-1.6 Ma	52.69	2.39	15.21	10.67	0.13
UPV	GFP 89	7-10	Montiferro	Trachyte	3.9-1.6 Ma	57.33	1.09	19.15	4.45	0.13
UPV	GFP 51	7-10	Montiferro	Basanite	3.9-1.6 Ma	47.41	3.09	13.42	10.02	0.14
UPV	MGV 236A	6-10	Montiferro	Hawaiite	3.9-1.6 Ma	50.13	3.18	14.62	11.50	0.18
UPV	MAL 143	7-10	Logudoro	Hawaiite	3.1-0.1 Ma	49.28	2.65	13.97	10.52	0.16
UPV	MGV 62	9-10	Orosei Dorgali	Hawaiite	3.9-2.1 Ma	48.95	1.82	16.04	9.76	0.14

UPV	MGV 76	9-10	Orosei Dorgali	Alkali basalt	3.9-2.1 Ma	48.00	1.76	15.66	10.22	0.14
UPV	MGV 98	9-10	Orosei Dorgali	Hawaiite	3.9-2.1 Ma	49.54	1.78	16.08	9.50	0.13
UPV	MGV 51	9-10	Orosei Dorgali	Basaltic Andesite	3.9-2.1 Ma	53.05	1.60	16.82	10.08	0.13
UPV	MGV 223	6-10	Orosei Dorgali	Alkali Basalt	3.9-2.1 Ma	51.40	2.12	14.96	11.26	0.15
UPV	MAL 32	9-10	Oristano Gulf (Capo Frasca)	Basaltic Andesite	4.8-3.2 Ma	54.51	1.48	15.47	10.87	0.12
UPV	MGL 23	6-10	Gerrei	Hawaiite	3.8-2.1 Ma	49.28	1.91	14.12	10.14	0.16
UPV	MGV 238	6-10	Santu Lussurgiu	Hawaiite	3.7-3.5 Ma	50.10	2.40	14.18	11.45	0.15

Sheet1

MgO	CaO	Na_2O	K_2O	P_2O_5	LOI	Sum	Mg#	$^{87}Sr/^{86}Sr_i$	ε_{Sr}	$^{143}Nd/^{144}Nd_i$	ε_{Nd}	$^{206}Pb/^{204}Pb_i$	$^{207}Pb/^{204}Pb_i$	$^{208}Pb/^{204}Pb_i$
8.98	12.76	1.79	0.51	0.23		100.00	0.64	0.70426	-2.7	0.512710	1.4	18.71	15.64	38.66
11.02	11.81	2.14	0.45	0.28		100.00	0.70	0.70398	-6.7	0.512710	1.4	18.69	15.62	38.55
4.19	**8.67**	**2.33**	**1.37**	**0.12**	**1.59**	**100.00**	**0.53**					**18.67**	**15.66**	**38.70**
0.86	**2.59**	**2.83**	**4.13**	**0.13**	**2.66**	**100.00**	**0.30**	**0.70627**	**25.8**	**0.512440**	**-3.9**	**18.70**	**15.67**	**38.80**
0.32	**1.04**	**3.56**	**5.43**	**0.07**	**1.57**	**100.00**	**0.22**	**0.70693**	**35.2**	**0.512540**	**-2.0**	**18.66**	**15.61**	**38.61**
0.16	**0.57**	**3.84**	**5.37**	**0.02**	**1.07**	**100.00**	**0.13**	**0.70554**	**15.5**	**0.512650**	**0.2**	**18.80**	**15.66**	**38.85**
0.19	**0.00**	**4.21**	**5.26**	**0.02**	**1.16**	**100.00**	**0.12**					**18.83**	**15.63**	**38.83**
0.27	**0.02**	**4.11**	**5.16**	**0.02**	**0.94**	**100.00**	**0.16**	**0.70502**	**8.1**	**0.512610**	**-0.6**	**18.82**	**15.64**	**38.84**
0.10	**0.51**	**4.09**	**5.53**	**0.02**	**1.20**	**100.00**	**0.10**					**18.70**	**15.60**	**38.62**
0.04	**0.00**	**4.04**	**4.44**	**0.03**	**0.10**	**100.00**	**0.02**	**0.70534**	**12.7**	**0.512730**	**1.8**	**18.83**	**15.64**	**38.79**
0.45	**0.70**	**3.44**	**6.49**	**0.02**	**1.71**	**100.00**	**0.29**	**0.70704**	**36.8**	**0.512530**	**-2.1**	**18.70**	**15.67**	**38.79**
0.01	**0.00**	**3.95**	**4.82**	**0.01**	**1.77**	**100.00**	**0.01**	**0.70358**	**-12.4**	**0.512670**	**0.6**	**18.59**	**15.59**	**38.54**
0.16	**0.69**	**3.20**	**5.58**	**0.03**	**1.09**	**100.00**	**0.13**					**18.71**	**15.66**	**38.76**
0.12	**0.12**	**3.84**	**4.88**	**0.01**	**1.16**	**100.00**	**0.08**	**0.70560**	**16.3**	**0.512610**	**-0.6**	**18.86**	**15.66**	**38.94**
3.58	**9.34**	**2.26**	**0.93**	**0.16**	**2.96**	**100.00**	**0.47**					**18.52**	**15.64**	**38.56**
3.01	**10.51**	**2.10**	**0.74**	**0.18**	**2.10**	**100.00**	**0.40**	**0.70590**	**20.6**	**0.512410**	**-4.5**	**18.48**	**15.65**	**38.62**
2.87	**9.21**	**2.21**	**1.18**	**0.15**	**2.74**	**100.00**	**0.41**	**0.70710**	**37.6**	**0.512370**	**-5.3**	**18.47**	**15.60**	**38.52**
9.38	10.15	1.98	0.55	0.09		100.00	0.68	0.70625	25.6	0.512600	-0.8	18.61	15.65	38.70
7.73	10.00	2.29	0.68	0.08		100.00	0.61	0.70542	13.8	0.512700	1.2	18.70	15.66	38.75
11.48	**8.45**	**1.86**	**0.97**	**0.18**		**100.00**	**0.71**	**0.70758**	**44.4**			**18.64**	**15.66**	**38.81**
10.03	**8.91**	**2.06**	**1.10**	**0.16**		**100.00**	**0.68**	**0.70715**	**38.3**	**0.512423**	**-4.2**	**18.69**	**15.66**	**38.85**
13.41	**9.88**	**1.52**	**0.39**	**0.11**		**100.00**	**0.74**	**0.70575**	**18.4**	**0.512641**	**0.0**	**18.70**	**15.65**	**38.71**
9.55	**9.66**	**1.93**	**0.80**	**0.11**		**100.00**	**0.70**	**0.70884**	**62.3**	**0.512289**	**-6.8**			
11.91	**9.62**	**1.75**	**0.21**	**0.16**		**100.00**	**0.71**	**0.70691**	**34.9**			**18.66**	**15.66**	**38.81**
8.82	**9.76**	**1.98**	**0.99**	**0.16**		**100.00**	**0.67**	**0.70670**	**31.9**	**0.512484**	**-3.0**	**18.63**	**15.65**	**38.79**
0.60	1.53	3.02	4.89	0.05	3.45	103.45	0.37	**0.70676**	**32.7**	**0.512417**	**-4.4**	**18.68**	**15.63**	**38.72**
1.52	3.67	3.00	4.20	0.13	2.56	102.49	0.48	**0.70681**	**33.6**	**0.512424**	**-4.2**	**18.68**	**15.64**	**38.74**

2.51	5.24	3.77	1.67	0.30		100.00	0.62	**0.70685**	**34.0**	**0.512279**	**-7.0**	**18.45**	**15.64**	**38.87**
1.20	3.76	2.55	2.43	0.07	7.42	107.41	0.41	**0.70780**	**47.5**	**0.512497**	**-2.8**			
5.25	8.73	2.56	1.52	0.21	1.48	101.43	0.54	**0.70611**	**23.6**	**0.512511**	**-2.5**	**18.56**	**15.61**	**38.47**
0.81	2.77	3.16	4.46	0.12	1.33	101.26	0.31	**0.70766**	**45.5**	**0.512329**	**-6.1**	**18.63**	**15.63**	**38.71**
3.67	4.92	2.76	3.57	0.17	2.46	102.41	0.62	**0.70878**	**61.5**	**0.512280**	**-7.0**	**18.65**	**15.62**	**38.74**
0.73	2.07	3.47	4.28	0.07	4.94	104.87	0.29	**0.70612**	**23.7**	**0.512499**	**-2.8**			
1.39	2.20	2.63	4.07	0.04	5.77	105.77	0.50	**0.70733**	**40.8**					
2.69	9.83	2.94	1.14	0.23	0.43	100.39	0.39	**0.70617**	**24.4**					
0.35	2.03	2.34	3.97	0.07	1.81	101.77	0.22	**0.70720**	**39.0**					
6.45	**12.23**	**2.71**	**0.29**	**0.29**		**100.00**	**0.55**	**0.70435**	**-1.4**	**0.512579**	**-1.2**	**18.68**	**15.62**	**38.69**
1.55	2.66	3.64	4.45	0.13	5.47	105.38	0.40	**0.70639**	**27.5**	**0.512410**	**-4.5**			
0.58	1.48	3.66	4.55	0.08	1.38	101.32	0.25	**0.70671**	**32.0**	**0.512468**	**-3.4**			
0.50	2.04	3.61	4.12	0.10	2.21	102.14	0.20	**0.70659**	**30.4**	**0.512461**	**-3.5**			
10.95	**10.66**	**1.17**	**0.51**	**0.08**		**100.00**	**0.71**	**0.70552**	**15.2**	**0.512683**	**0.8**	**18.67**	**15.64**	**38.69**
1.26	3.41	4.81	4.22	0.37		100.00	0.30	0.70487	6.0	0.512710	1.4	18.84	15.66	38.98
4.24	5.93	3.60	3.23	0.84		100.00	0.52	0.70437	-1.2	0.512746	2.1	18.93	15.66	39.06
7.55	10.37	3.49	2.23	0.39		100.00	0.59	0.70401	-6.2	0.512850	4.1	19.23	15.64	39.10
5.03	8.58	3.46	2.49	0.77		100.00	0.50	0.70315	-18.5	0.512890	4.9	19.42	15.66	39.13
0.50	**0.58**	**5.18**	**6.93**	**0.11**	**1.35**	**100.15**	**0.30**	**0.70548**	**14.7**	**0.512761**	2.4	**18.94**	**15.62**	**38.92**
0.51	**0.48**	**5.20**	**6.83**	**0.13**	**1.95**	**100.18**	**0.30**	**0.70547**	**14.5**	**0.512745**	2.0	**18.94**	**15.62**	**38.94**
3.00	4.32	5.70	3.38	0.98	1.36	100.18	0.45	0.70489	6.2	0.512771	2.6			
0.10	0.60	6.24	6.11	0.08	0.32	100.02	0.06	0.70516	10.1	0.512750	2.1			
5.91	7.26	2.88	2.79	0.57		100.00	0.54	0.70428	-2.3	0.512632	-0.2	17.98	15.56	37.98
6.61	7.01	3.79	2.88	0.64		102.02	0.58	0.70474	4.1					
0.87	3.18	5.59	5.33	0.29		97.42	0.31	0.70502	8.2	0.512459	-3.5			
10.07	8.28	5.43	1.32	0.87		100.04	0.69	0.70434	-1.5	**0.512591**	**-1.0**			
4.85	8.49	4.32	1.61	1.11		100.00	0.49	0.70435	-1.4	0.512561	-1.5	17.64	15.57	37.92
8.92	8.37	4.62	1.01	0.51		100.00	0.66	0.70437	-1.2	0.512598	-0.8	18.07	15.58	38.23
9.69	8.00	3.40	1.80	0.41		100.00	0.69	0.70451	0.9	0.512550	-1.8			

10.91	8.49	3.61	0.82	0.38		100.00	0.71	0.70442	-0.4	0.512571	-1.3	17.86	15.60	37.94
10.02	7.37	3.33	1.86	0.39		100.00	0.70	0.70446	0.1	0.512528	-2.2			
6.09	7.90	3.42	0.72	0.19		100.00	0.58	0.70465	2.8	0.512470	-3.3	17.83	15.59	38.02
6.61	8.39	2.83	1.78	0.50		100.00	0.57	0.70437	-1.1	0.512570	-1.4	17.84	15.55	37.92
6.26	6.58	3.83	0.71	0.17		100.00	0.56	0.70495	7.2	0.512320	-6.2	17.67	15.57	37.84
9.97	7.75	4.28	1.41	0.98		100.00	0.69	0.70433	-1.7	0.512580	-1.2	17.87	15.58	37.84
7.60	8.14	3.83	1.54	0.61		100.00	0.60	0.70434	-1.6	0.512568	-1.4	18.01	15.61	38.15

Δ7/4	Δ8/4	$^{207}Pb/^{206}Pb$	$^{208}Pb/^{206}Pb$	$\delta^{18}O$	$^{176}Hf/^{177}Hf$	$^{187}Os/^{188}Os_i$	Sc	V	Cr	Co	Ni	Rb	Sr	Y
12.5	41.9	0.84	2.07	**5.41 (ol)**	**0.282893**			311	345	40.9	82	10.7	371	16
10.2	32.8	0.84	2.06	**5.58 (ol)**	**0.282928**	**2.420**		309	756	52.7	220	7.8	450	17
14.1	**49.2**	**0.84**	**2.07**				**23.4**	**197**	**50**	**22**	**20**	**58**	**346**	**19**
15.5	**56.7**	**0.84**	**2.07**				**12.7**	**10**		**1**		**193**	**76**	**61**
9.6	**42.5**	**0.84**	**2.07**				**8.5**	**14**		**2**		**198**	**114**	**44**
13.3	**49.5**	**0.83**	**2.07**				**5.4**	**10**		**2**		**197**	**72**	**62**
9.8	**44.0**	**0.83**	**2.06**				**4.5**					**254**	**12**	**64**
10.4	**46.3**	**0.83**	**2.06**				**2.6**					**246**	**10**	**69**
7.8	**38.7**	**0.83**	**2.07**				**3.6**	**8**		**1**		**204**	**97**	**26**
11.0	**40.3**	**0.83**	**2.06**				**5.0**					**280**	**5**	**133**
15.4	**55.5**	**0.84**	**2.07**				**9.5**	**12**		**1**		**222**	**98**	**49**
8.8	**43.2**	**0.84**	**2.07**				**2.2**					**312**	**2**	**66**
13.6	**52.3**	**0.84**	**2.07**				**9.1**	**12**				**213**	**47**	**44**
12.7	**50.8**	**0.83**	**2.06**				**3.2**					**236**	**7**	**61**
14.0	**53.7**	**0.84**	**2.08**				**31.0**	**203**		**20**		**23**	**358**	**21**
15.3	**64.5**	**0.85**	**2.09**				**37.1**	**301**	**40**	**22**		**23**	**426**	**21**
11.1	**56.0**	**0.84**	**2.09**				**32.1**	**249**		**18**		**32**	**359**	**21**
14.3	57.2	0.84	2.08	**6.43 (ol)**	**0.282877**			255	701	36.4	116	13.3	192	17.5
14.3	51.0	0.84	2.07		**0.283022**			299	202	42.5	127	21.7	186	19.4
15.1	**65.1**	0.84	2.08				**38**	**228.3**	**593**	**40.3**	**170**	**29.0**	**156.4**	**18.1**
14.6	**62.3**	0.84	2.08	**6.21 (ol)**			**40**	**233.3**	**580**	**42.8**	**178**	**39.7**	**156.7**	**17.8**
13.5	**48.0**	0.84	2.07				**39**	**230.2**	**820**	**45.7**	**199**	**15.3**	**146.7**	**15.6**
				7.02 (cpx)				**192**	**398**	**30.8**	**96**	**26.1**	**189**	**19.1**
14.6	**62.0**	0.84	2.08		**0.282814**		**36**	**223.7**	**596**	**40.6**	**172**	**10.6**	**187.1**	**12.6**
14.4	**64.0**	0.84	2.08				**39**	**242.2**	**357**	**36.4**	**117**	**21.8**	**183.8**	**15.2**
11.0	**50.7**	**0.84**	**2.07**				3			1		179.0	139	24
12.2	**53.6**	**0.84**	**2.07**				10	53	50	7	30	136.0	249	24

14.9	**93.7**	**0.85**	**2.11**				12	51.51	7	2.8		28.9	392	15
							10	7		2		214.0	457	44
10.3	**40.1**	**0.84**	**2.07**				32	246		23		35.0	285	26
11.8	**55.6**	**0.84**	**2.08**				9	49		8		161.0	182	26
10.7	**57.6**	**0.84**	**2.08**				15	70		9		118.0	265	26
							10	12		3		178.0	125	41
							10	23		2		129.0	135	37
							31	285		21		25.0	321	21
							6	25		2		128.0	182	20
10.5	**47.6**	**0.84**	**2.07**		**0.282776**		**53**	**442**	**37**	**39.5**	**34**	**4.4**	**480.4**	**19.9**
							11	21		4		210.0	238	27
							12	12		2		145.0	114	41
							12	25		2		141.0	139	33
12.2	**48.8**	**0.84**	**2.07**		**0.283021**	**0.1317**	**47**	**256**	**405**	**42**	**130**	**11.6**	**169**	**14.1**
12.4	57.2	0.83	2.07	**7.17 (pl)**				29	1	8	6	99.0	321	45.7
11.8	54.4	0.83	2.06	**5.43 (ol)**	**0.282865**		11	79	37	18	31	64.8	593	33.5
6.4	22.4	0.81	2.03		**0.282944**	**0.1842**	20	254	139		52	53.0	884	30.0
6.4	2.4	0.81	2.01		**0.283037**	**0.1983**	18	243	141		85	44.5	812	25.2
7.4	**39.5**	**0.82**	**2.05**				**4**					**249.0**	**65**	**37.0**
7.9	**41.0**	**0.82**	**2.06**									**245.0**	**50**	**34.0**
					0.282866			76		58	3	88.3	809	32.3
					0.282895			3		51	6	253.6	43	40.2
12.4	61.8	0.87	2.11		**0.282772**	**0.1566**	7.9	172	117	39	157	50.0	883	24.3
				5.51 (ol)		**0.1255**	7.16	18.96	179		10	12.0	2.43	1.4
				5.41 (cpx)			10.96	27.80			24	2.0	7.46	2.4
				5.93 (cpx)			9.29	21.06	414		17	18.0	4.56	1.7
16.6	97.1	0.88	2.15		**0.282592**	**0.2945**	19	238	54		52	67.1	1561	36.9
13.0	75.1	0.86	2.12			**0.1294**	18	168	321	40	232	46.8	1,140	21.4
				5.37 (ol)				187	376	47	228	32.8	682	19.7

16.9	72.2	0.87	2.12		**0.282791**	**0.1475**		193	386	54	295	25.7	681	18.3
				5.45 (ol)				165	414	46	283	33.5	666	19.6
16.6	83.7	0.87	2.13			**1.3301**		157	235	44	138	7.8	505	19.2
12.5	72.4	0.87	2.13			**0.4230**	22	175	229		150	13.8	589	22.0
16.5	85.3	0.88	2.14	**6.74 (cpx)**	**0.282620**		17.00	143	246	37	125	14.1	532	17.9
15.2	60.8	0.87	2.12	**6.67 (pl)**	**0.282742**	**0.1313**	17	178	349		248	45.0	833	18.0
16.5	74.9	0.87	2.12	**5.98 (ol)**		**0.1583**	20	199	301		196	60.5	821	24.3

Zr	Nb	Cs	Ba	La	Ce	Pr	Nd	Sm	Eu	Gd	Tb	Dy	Ho	Er	Tm	Yb
33.5	1.8	0.20	0.01	4.39		1.6	7.8	2.44	0.82	2.56	0.43	2.77	0.56	1.51	0.23	
35.2	1.9	0.15	0.1	4.53		1.8	9.2	2.59	0.84	2.49	0.46	2.84	0.64	1.57	0.27	
98.0	**5**	**2.20**	**309**	**14.8**	**30.3**	**3.9**	**16.2**	**3.7**	**1.0**	**3.9**	**0.6**	**3.6**	**0.7**	**2.1**	**0.3**	**2.1**
493.0	**51**	**0.60**	**704**	**55.6**	**97.3**	**12.1**	**43.5**	**8.7**	**1.2**	**9.0**	**1.6**	**9.3**	**1.9**	**5.9**	**0.9**	**6.5**
565.0	**49**	**1.90**	**1,210**	**56.6**	**113.0**	**13.5**	**48.7**	**9.7**	**1.8**	**8.5**	**1.4**	**7.9**	**1.5**	**4.6**	**0.7**	**4.7**
503.0	**53**	**0.60**	**704**	**56.6**	**99.6**	**12.2**	**44.2**	**8.7**	**1.2**	**9.4**	**1.6**	**9.5**	**2.0**	**6.1**	**0.9**	**6.4**
742.0	**94**	**9.00**	**73**	**82.3**	**164.0**	**20.3**	**72.3**	**14.5**	**0.2**	**12.3**	**2.1**	**12.3**	**2.4**	**7.3**	**1.2**	**7.9**
730.0	**104**	**5.10**	**74**	**97.7**	**167.0**	**23.5**	**83.4**	**16.2**	**0.2**	**13.5**	**2.3**	**13.0**	**2.6**	**7.6**	**1.2**	**7.8**
498.0	**52**	**1.40**	**780**	**56.7**	**129.0**	**15.4**	**51.1**	**10.3**	**1.3**	**6.6**	**1.2**	**6.8**	**1.2**	**3.4**	**0.6**	**3.9**
1,360.0	**169**	**1.60**	**5**	**149.0**	**258.0**	**35.1**	**127.0**	**26.5**	**0.9**	**24.5**	**4.4**	**25.8**	**5.0**	**14.8**	**2.2**	**14.6**
537.0	**49**	**2.80**	**1,210**	**57.4**	**107.0**	**14.4**	**52.2**	**10.3**	**1.7**	**8.9**	**1.4**	**8.3**	**1.6**	**4.9**	**0.8**	**5.1**
852.0	**109**	**6.00**		**78.4**	**145.0**	**19.2**	**68.3**	**14.0**	**0.1**	**12.4**	**2.2**	**12.5**	**2.5**	**7.4**	**1.2**	**8.2**
414.0	**36**	**3.90**	**781**	**55.0**	**108.0**	**13.3**	**50.0**	**10.4**	**1.3**	**9.1**	**1.5**	**8.1**	**1.6**	**4.7**	**0.7**	**4.8**
735.0	**105**	**4.20**	**22**	**77.6**	**148.0**	**18.4**	**65.2**	**12.9**	**0.1**	**11.2**	**2.0**	**11.3**	**2.2**	**6.6**	**1.0**	**6.9**
105.0	**6**	**2.40**	**308**	**13.9**	**31.0**	**4.2**	**17.9**	**4.3**	**1.2**	**4.5**	**0.7**	**4.2**	**0.8**	**2.4**	**0.4**	**2.4**
104.0	**6**		**258**	**13.6**	**28.9**	**4.0**	**16.7**	**4.0**	**1.1**	**4.2**	**0.7**	**4.0**	**0.8**	**2.3**	**0.4**	**2.3**
107.0	**7**	**0.60**	**400**	**14.9**	**31.0**	**4.2**	**17.7**	**4.1**	**1.2**	**4.2**	**0.7**	**3.9**	**0.8**	**2.3**	**0.4**	**2.3**
50.4	2.4	0.36		6.55		1.9	7.9	2.2	0.78	2.58	0.43	2.91	0.6	1.55	0.24	
42.5	1.5	0.54		6.27		1.8	8.0	2.17	0.75	2.42	0.48	3.05	0.65	1.68	0.29	
77.7	**3.6**	**1.49**	**225**	**11.57**	**23.8**	**3.0**	**12.0**	**2.87**	**0.79**	**2.94**	**0.48**	**3.02**	**0.62**	**1.8**	**0.26**	**1.81**
66.1	**3.2**	**1.57**	**202**	**10.22**	**20.9**	**2.7**	**11.2**	**2.71**	**0.73**	**2.76**	**0.45**	**2.84**	**0.58**	**1.69**	**0.25**	**1.72**
55.0	**1.3**	**0.69**		**4.42**	**9.6**	**1.3**	**5.9**	**1.69**	**0.57**	**1.91**	**0.41**	**2.13**	**0.45**	**1.3**	**0.24**	**1.61**
85.2	**5.3**	**1.00**		**14.8**		**3.6**	**13.9**	**3.10**	**0.886**	**3.09**	**0.55**	**3.41**	**0.71**	**1.93**	**0.298**	
34.6	**2.4**	**4.60**	**145**	**8.05**	**16.7**	**2.2**	**9.1**	**2.33**	**0.69**	**2.5**	**0.33**	**2.66**	**0.55**	**1.59**	**0.2**	**1.33**
50.3	**2.1**	**3.24**	**179**	**7.21**	**15.2**	**2.0**	**8.5**	**2.18**	**0.68**	**2.42**	**0.4**	**2.52**	**0.53**	**1.53**	**0.23**	**1.58**
165.0	11.0	6.60	486	38.5	73.8	7.5	26.1	4.5	0.81	3.8	0.6	3.9	0.8	2.5	0.4	2.8
216.0	15.0	5.00	572	34.2	64.0	7.4	25.2	4.9	1.11	4.3	0.7	3.9	0.8	2.4	0.38	2.5

132.2	9.5	1.20	423	26.79	51.4	6.0	22.1	3.97	1.04	3.11	0.46	2.62	0.51	1.46	0.22	1.57
215.0	13.0	171.00	569	32.2	61.7	7.7	29.9	6.8	1.4	7.2	1.2	7.3	1.5	4.6	0.72	4.7
82.0	7.0	2.30	195	14.6	30.7	3.9	16.1	4.1	1.26	4.3	0.7	4.6	0.9	2.8	0.42	2.8
206.0	12.0	5.00	654	34.4	67.8	7.1	25.3	5.1	1.02	4.6	0.7	4.4	0.9	2.6	0.42	2.8
227.0	11.0	3.20	572	33.5	64.8	7.3	27.2	5.6	1.44	5.3	0.8	4.7	0.9	2.7	0.42	2.8
254.0	14.0	9.40	516	31	61.6	7.1	27.6	6	1.24	6.1	1.1	6.9	1.4	4.3	0.68	4.5
257.0	13.0	8.60	842	29.4	59.0	6.2	24.4	5.6	1.03	5.4	0.9	5.8	1.2	3.8	0.6	3.9
67.0	5.0	1.40	185	11.4	24.0	3.0	12.8	3.4	1.13	3.8	0.7	3.9	0.8	2.3	0.35	2.3
168.0	9.0	4.30	470	29.2	56.5	6.3	22.1	4.3	1.05	3.9	0.6	3.4	0.7	2.1	0.34	2.2
45.2	**2.6**	**0.92**	**86**	**7.2**	**16.5**	**2.4**	**11.2**	**3.17**	**1.07**	**3.46**	**0.57**	**3.57**	**0.72**	**2.01**	**0.28**	**1.87**
243.0	15.0	13.40	545	39.5	77.0	8.4	30.8	6	1.44	5.5	0.9	5.3	1.1	3.2	0.5	3.3
256.0	18.0	3.40	562	38.1	69.3	8.3	32.4	7.5	1.38	7.1	1.3	7.8	1.6	4.8	0.7	4.5
235.0	17.0	3.20	545	28.4	50.9	6.7	25.3	5.4	1.4	5.2	0.9	5.3	1.1	3.2	0.48	3.2
39.0	**1.3**	**0.65**		**4.2**	**9.1**	**1.3**	**5.9**	**1.8**	**0.49**	**1.92**	**0.36**	**2.27**	**0.49**	**1.42**	**0.21**	**1.34**
508.0	74.4		1,022	66	130.4		57.8									
312.7	54.2	1.42	1,023	51.00	105.0	12.7	50.0	9.80	3.16	8.00	1.21	6.50	1.21	3.10	0.42	2.78
245.0	77.0		702	60	95.0											
211.7	70.9		655	59	86.0		43.9									
939.0	**149.0**	**6.00**	**138**	**95.4**	**177.0**	**19.5**	**64.1**	**10.5**	**0.9**	**7.5**	**1.1**	**6.7**	**1.4**	**4.0**	**0.6**	**4.4**
899.0	**142.0**	**6.00**	**109**	**101.0**	**179.0**	**20.5**	**66.6**	**10.9**	**1.0**	**7.4**	**1.2**	**6.5**	**1.3**	**3.7**	**0.6**	**4.1**
427.6	90.3	4.54	950	78.7	162.5	18.1	68.9	12.2	3.3	9.2	1.3	6.5	1.1	3.0	0.4	2.7
1,007.0	185.5	4.64	93	123.2	227.6	23.5	74.9	11.6	0.9	8.3	1.3	7.1	1.3	4.0	0.6	4.5
253.3	55.2	0.51	1,150	48.4	81.4	10.7	40.3	7.45	2.43	6.65	0.93	4.61	0.82	2.00	0.238	1.52
39.7	39.8		1,343	44.49	86.3	51.0	122.0	947	2.37	7.48	4.70	4.29	0.71	1.78	1.09	106
102.2	78.9		884	116.85	246.6	168.0	1.0	1396	3.20	12.10	11.75	6.44	1.02	2.82	2.66	67
73.7	60.4		2,127	75.43	150.2	41.0	265.0	1084	2.87	10.87	7.57	5.51	0.86	2.22	1.83	77
681.4	106.9		1,537	124	212.7		95.7									
298.5	69.6	0.71	1,230	65.1	116.1	13.7	48.1	7.96	2.55	6.67	0.92	4.38	0.77	2.00	0.277	1.56
174.2	35.5		743	36	60.4		28.0									

155.8	31.3		689	27	60.5		28.0									
184.6	36.0		721	35	68.9		29.2									
112.8	14.7		387	18	39.8		19.1									
164.5	42.5		767	28	60.5		34.4									
86.0	9.8	0.27	311	14.0	27.3	3.8	18.1	4.60	1.65	4.20	0.63	3.28	0.64	1.44	0.21	1.20
242.0	47.0		1,063	39	85.0		40.0									
201.5	55.7		1,115	49	83.5		29.2									

Lu	Hf	Ta	Pb	Th	U	Cu	Zn	Ga	Re (ppb)	Os (ppb)
									1.02	**0.11**
0.3	**2.4**	**0.3**	**9**	**3.6**	**1.0**	**50**	**90**	**17**		
1.1	**10.3**	**4.2**	**25**	**21.8**	**5.9**		**90**	**18**		
0.8	**11.7**	**3.6**	**20**	**19.5**	**4.8**		**60**	**18**		
1.1	**10.3**	**4.4**	**25**	**22.2**	**6.0**		**90**	**18**		
1.3	**16.2**	**7.7**	**30**	**27.0**	**6.5**		**140**	**26**		
1.3	**15.8**	**7.7**	**39**	**26.7**	**5.4**		**130**	**26**		
0.6	**10.3**	**4.3**	**42**	**21.3**	**4.0**		**60**	**19**		
2.3	**28.6**	**13.4**	**34**	**34.4**	**5.6**		**240**	**30**		
0.8	**11.5**	**3.7**	**28**	**20.5**	**5.6**		**70**	**18**		
1.4	**19.7**	**9.3**	**37**	**38.8**	**9.8**		**170**	**26**		
0.8	**9.4**	**2.8**	**29**	**20.1**	**5.4**		**60**	**18**		
1.1	**16.0**	**7.5**	**31**	**26.0**	**6.6**		**120**	**25**		
0.4	**2.5**	**0.4**	**7**	**3.1**	**0.6**	**30**	**120**	**19**		
0.4	**2.5**	**0.4**	**7**	**3.3**	**0.7**	**40**	**120**	**19**		
0.4	**2.6**	**0.4**	**8**	**4.1**	**0.8**	**30**	**120**	**19**		
0.29	**2.14**	**0.29**	**7.49**	**3.8**	**0.85**	**102.9**	**80.38**	**14.85**		
0.28	**1.89**	**0.25**	**6.52**	**3.83**	**0.84**	**90.58**	**82.52**	**14.69**		
0.22	**1.07**	**0.19**	**3.63**	**2.39**	**0.54**	**91.12**	**75.52**	**12.32**		
0.26	**1.62**	**0.11**	**4.88**	**1.34**	**0.4**	**91.36**	**73.66**	**13.81**		
0.25	**1.44**	**0.17**	**4.87**	**2.41**	**0.54**	**94.68**	**81.01**	**15.19**		
0.45	4.8	1	22	14.3	3.5		50			
0.4	5.6	1	58	14.4	3.4	20	60			

0.25	3.56	0.76	9.72	6.83	0.9		35	18.13		
0.71	5.8	1	37	10	2.7		80			
0.43	2.5	0.4	8	2.8	0.7	70	90			
0.44	5.5	0.9	39	14.2	3.2	30	70			
0.41	5.8	0.8	22	11.2	2.5	20	60			
0.68	6.9	1.1	18	10.5	2.9	10	70			
0.58	6.6	0.9	33	10.5	2.4	10	40			
0.34	1.9	0.3	6	2.2	0.5	70	80			
0.34	4.3	0.6	37	9.5	2.1		40			
0.29	**1.41**	**0.21**	**2.79**	**0.97**	**0.27**	**84.63**	**103**	**19.39**		
0.49	6.4	1.2	20	16.6	4.2	30	80			
0.68	6.9	1.1	21	11.8	2.6		60			
0.52	6.4	1.1	16	11.9	2.8		70			
0.2		**0.1**	**1.57**	**1.04**	**0.28**		**72.56**		**0.048**	**0.021**
						12	105			
0.39	6.90	3.50	3.47	7.80	1.92		75			
							93		**0.453**	**0.044**
							92		**0.238**	**0.018**
0.8	**16.5**	**12.6**	**13**	**27.3**	**7.0**		**90.0**	**23.0**		
0.7	**15.7**	**11.9**	**11**	**26.6**	**6.7**		**90.0**	**23.0**		
0.4	8.3	7.0		10.5	3.0	8.1	146.5	23.4		
0.7	19.5	15.0		38.5	9.8		84.6	26.6		
0.204	6.2	3.67	9	6.68	1.12	46	114		**0.148**	**0.028**
0.19	4.84	0.83		0.23	191		214			
0.33	13.33	1.24		0.36	45		611			
0.24	7.41	1.08		0.28	255		353			
							130		**0.092**	**0.030**
0.219	7.3	4.54	6	9.40	1.72	39	93		**0.072**	**0.083**
						43	91			

						47	91		**0.188**	**0.180**
						47	91			
						46	105		**0.185**	**0.017**
							93		**0.100**	**0.011**
0.16	2.37	0.65	1.41	1.60	0.34		112			
							95		**0.117**	**0.222**
							96		**0.11**	**0.05**

Highlights

- The Cenozoic magmatism in Sardinia can be grouped into three main phases.
- Sr-Nd-Pb-Hf-O-Hf isotopic ratios discrinate well these three rock groups.
- The subduction-related signal may be not directly related to Apennine subduction.
- The origin of the “anorogenic” magmatism remains not totally understood.
- The youngest rocks are the most peculiar within the entire circum-mediterranean.